Local synaptic inhibition mediates cerebellar pattern separation necessary for learned sensorimotor associations

Elizabeth A. Fleming[1], Michael R. Tadross[1,2] and Court Hull[1]

[1]*Department of Neurobiology, Duke University Medical School, Durham, United States*
[2]*Department of Biomedical Engineering, Duke University, Durham, United States*

Correspondence:

Dr. Court Hull
Duke University Medical School
Dept. of Neurobiology
311 Research Drive
Durham, NC 27710

Email: Hull@neuro.duke.edu
Phone: 919-613-0927

Dr. Elizabeth Fleming
University of North Carolina Chapel Hill
Neuroscience Center
116 Manning Drive
Chapel Hill, NC 27599

lizflem@email.unc.edu
919-966-6329

Acknowledgements:

This work was supported by grants from the NIH NINDS (CH: 5R01NS096289-02, EF: 1F31NS113742-01A1). We thank Drs. Stephen Lisberger, Lindsey Glickfeld, John Pearson, and Nicole Calakos for input throughout the project, as well as Drs. Javier Medina and Shane Heiney for input specific to eyelid conditioning experiments and analysis, and Dr. Brenda Shields for technical assistance with DART reagents.

Abstract

The cerebellar cortex plays a key role in generating predictive sensorimotor associations. To do so, the granule cell layer is thought to establish unique sensorimotor representations for learning. However, how this is achieved, and how granule cell population responses contribute to behavior, has remained unclear. To address these questions, we have used *in vivo* calcium imaging and granule cell specific pharmacological manipulation of synaptic inhibition in awake, behaving mice. We find that inhibition sparsens and thresholds sensory responses, limiting overlap between sensory ensembles, and preventing spiking in many granule cells that receive excitatory input. Moreover, we find that inhibition can be recruited in a stimulus-specific manner to powerfully decorrelate multisensory ensembles. Consistent with these results, we find that granule cell inhibition is required for sensory discrimination in a cerebellum-dependent behavior. These data thus reveal new mechanisms for granule cell layer pattern separation beyond those envisioned by classical models.

Introduction

Associative learning is an essential process linking sensation and action, providing a key mechanism to modify behavior. The cerebellum plays a central role in associative sensorimotor learning, both for generating coordinated movements and cognitive processes[1, 2]. To do so, the cerebellum receives excitatory mossy fiber input from diverse sources[3] that transmit sensory, motor, and cognitive information to granule cells in the granule cell layer[4]. Granule cells must integrate and relay these signals to Purkinje cells, the output neurons of the cerebellar cortex, in a manner that establishes unique sensorimotor representations necessary for associative learning and the expression of learned cerebellum-dependent behaviors.

Classical models speculate that unique granule cell representations are generated through a process of "pattern separation"[5, 6]. Expansion recoding is one mechanism thought to enable pattern separation, because mossy fiber inputs are distributed onto a population of granule cells that is ~100-fold larger than the number of mossy fiber inputs[6]. Because each granule cell receives ~4 inputs that can transmit the same or different modalities[7-10], random mixing is also thought to facilitate pattern separation. Another key mechanism proposed by classical theories is the thresholding of granule cell activity by local inhibitory interneurons in the granule cell layer called Golgi cells. Golgi cells exhibit spontaneous pacemaker activity, releasing GABA that acts continuously on granule cells to produce a tonic inhibitory current[11, 12]. This tonic inhibition regulates the spike threshold[13] and gain of granule cell responses[14]. In addition, Golgi cells receive feedforward excitation from mossy fibers and feedback excitation from granule cells, thus allowing them to respond dynamically to the inputs and outputs of the granule cell layer. Together, this tonic and phasic Golgi cell inhibition has long been hypothesized as necessary for creating sparse, non-overlapping granule cell population codes.

In contrast with the predictions of classical theories, modern calcium imaging approaches have shown that granule cell responses can be dense and redundant in some conditions[15-18]. These studies have indicated that complex behaviors requiring task engagement, learning, and

compound body movements likely to involve sensory, motor, cognitive, and efference copy signals can result in relatively widespread granule cell activity. In such cases, where there are many complex granule cell representations evolving across time, it has been challenging to disentangle discrete sensory representations and how they combine to form complex multisensory codes that remain dissociable for learning and behavior. Moreover, it has been difficult to test what mechanisms shape these sensory representations, as there has been a lack of tools for acute, cell type-specific manipulations of granule cell GABAergic inhibition. Thus, how the granule cell layer encodes discrete sensory input, how local synaptic inhibition contributes to such representations, and what role granule cell inhibition plays in cerebellum-dependent behavior have remained unclear.

To address these questions, we have measured cerebellar granule cell population responses in the presence and absence of synaptic inhibition. In response to discrete sensory input, we find that granule cell population activity is sparse and can be highly variable in terms of response probability, neural ensemble identity, and response timing across trials. Blocking synaptic inhibition onto granule cells dramatically enhances stimulus-evoked responses, revealing a large population of previously inactive cells, suggesting that thresholding is a key mechanism for sparsifying granule cell population ensembles. In addition, this thresholding establishes separate granule cell populations that can only respond to combined multisensory inputs, a property that would not be possible if ensemble sparsity were determined by inputs alone. Surprisingly, we also find that inhibition can be recruited in a stimulus-specific manner, further enhancing pattern separation by removing cells from multisensory ensembles that are part of unisensory ensembles. In support of our finding that synaptic inhibition plays a central role in granule cell layer pattern separation, we find that blocking inhibition onto granule cells impairs the expression of learned cerebellum-dependent sensorimotor discriminations. Together, these data reveal multiple distinct computations mediated by GABAergic inhibition onto granule cells that support pattern separation and behavior in a manner not predicted by classical models.

Results

Granule cell synaptic inhibition sparsens population-level sensory representations

To measure sensory-evoked activity in populations of cerebellar granule cells, we performed two-photon calcium imaging of GCaMP6f, which has been shown to report spiking in granule cells *in vitro*[16]. By crossing Ai148[19] and BACα6Cre-A transgenic mice[20], we observed dense labeling of granule cells, with only rare off-target labeling of Purkinje cells, which were excluded from imaging analysis (Methods, Supp. Fig. 1). We imaged activity in Crus I of the lateral cerebellum (Fig. 1) in response to auditory stimuli (Fig. 1c-g, pure tones: 1, 5 and 10 Hz at 68 and 72 dB; Supp. Fig. 2) and somatosensory stimuli (gentle orofacial air puffs: 10, 15 and 20 PSI; Supp. Fig. 3). In this region, *in vivo* recordings have identified that granule cells respond to these modalities[9, 21, 22]. Moreover, anatomical tracing has revealed that Crus I is a major cerebellar destination of both auditory and somatosensory inputs[23].

Because our goal was to measure discrete sensory responses, and Crus I also receives input related to whisking and likely other movements[24-28], we took multiple steps to isolate sensory-related granule cell activity. First, animals were habituated to orofacial airpuffs, such that they produced reflexive whisker movements on only a small minority of trials. Second, high-speed

video was used to detect whisker and facial movements between trials and isolate responses related to these movements[29] (Supp. Fig. 4). Third, we controlled for spontaneous and reactive body movements using a sensitive piezo vibration sensor[30, 31] (Figure 1a, Supp. Fig. 5). Together, these approaches enabled us to discard trials with body movement and demonstrate that whisking-related activity does not contaminate sensory responses (Supp. Figure 4, 5; see Methods).

In control conditions, combining data across stimulus frequencies and intensities, we find that both auditory and somatosensory stimuli recruit population level granule cell activity in Crus I (Fig. 1). All stimuli evoke granule cell responses that begin near the time of stimulus onset (Fig 1c,h). For auditory stimuli, which could be delivered for a longer duration (1 s) than somatosensory stimuli, the mean responses of individual granule cells tile the duration of the stimulus window (Fig. 1c, 4a). Furthermore, many granule cells respond preferentially at the offset of the stimulus (Fig. 1c). Overall, granule cells in control conditions produce modest responses (Fig. 1d,e,l,j) occurring with a low probability (Figure 1f,k; auditory: 0.145 ± 0.003, n=3360; somatosensory: 0.056 ± 0.005, n=815) and small single trial amplitude (Fig. 1 g, l; auditory: 0.410 ± 0.008 ΔF/F, n = 1942; somatosensory: 0.532 ± 0.043, n = 118). These properties are consistent for all individual auditory and somatosensory stimuli tested (Supp. Fig. 2,3).

Both classical models[5, 6] and *in vivo* whole-cell recordings[13] have suggested that inhibition restricts granule cell sensory responses due to spike thresholding. Therefore, local inhibition could explain the low probability and amplitude of individual granule cell trial-by-trial responses. To test how local synaptic inhibition regulates sensory-evoked granule cell responses, we used the DART system (Drugs Acutely Restricted by Tethering)[32] to selectively block $GABA_A$ receptors on granule cells (Shields et al. 2022, bioRxiv, Fig. 1., Supp. Fig. 1,5,6). This system has been used to demonstrate block of GABAergic inhibition onto cerebellar granule cells *in vitro* (Shields et al. 2022, bioRxiv). Here, we expressed a GPI-anchored HaloTag Protein (HTP_{GPI}) in granule cells to acutely and cell type-specifically antagonize $GABA_A$ receptors upon infusion of gabazine.1$^{DART.2}$ (Fig. 1, "DART"). This manipulation dramatically alters responses to all sensory stimuli tested (Fig 1, Supp. Figs. 2,3), producing significantly larger mean population responses (Fig. 1 d-e,i-j), increased response probability (Figure 1f,k; auditory: 0.384 ± 0.003, n = 2220, $P < 0.0001$, paired t-test; somatosensory: 0.314 ± 0.008, n = 727, $P < 0.0001$, paired t-test), and increased amplitude of single trial responses (Figure 1g,l; auditory: 0.596 ± 0.019 ΔF/F, n = 1144, $P < 0.0001$, paired t-test; somatosensory: 0.876 ± 0.066, n = 165, $P < 0.0001$, paired t-test). These changes in single trial response probability and amplitude were observed across all individual variations of auditory and somatosensory stimuli tested (Supp. Fig 2-3).

In addition to changes in sensory evoked responses, we also observed a significant enhancement of spontaneous activity when inhibition was blocked (Fig. 1c,h, control F: 0.000 ± 0.000, DART F: 0.004 ± 0.001, n = 1616, $P < 0.0001$). This effect is consistent with previous data revealing that a non-specific block of GABAergic inhibition in the cerebellar cortex increases spontaneous granule cell spiking and can degrade the signal-to-noise ratio of sensory evoked responses[33].

To test the selectively of these effects, we used a variation of gabazine.1$^{DART.2}$ that cannot bind HTP (non-binding gabazine.1^{nbDART}, "nbDART") and a variation of HTP that cannot bind ligand (^{dd}HTP) (Shields et al. 2022, bioRxiv). Neither nbDART infused into animals expressing HTP, nor DART infused into animals expressing ^{dd}HTP significantly changes auditory or somatosensory

responses (Supp. Fig. 6,7). Together, these results are consistent with a central role of GABAergic inhibition in enforcing granule spike thresholds to restrict population activity, maintaining sparsity of spiking both within and across trials.

Importantly, many granule cells that are silent in control conditions become responsive after blocking synaptic inhibition, resulting in a dramatic increase in the number of granule cells responsive to both auditory and somatosensory stimulation (Fig. 1c,h, Fig. 2a,b). We therefore compared the number of responsive cells to a conservative estimate of the total cells present in our field of view (based on the size of ROIs detected with our analysis, see Methods). This allowed us to estimate that under baseline conditions, approximately 5.2 ± 0.5% of granule cells in our field of view responded to any individual auditory stimulus and 1.1 ± 0.2% of granule cells responded to any individual somatosensory stimulus (Figure 2a,b). Following block of synaptic inhibition, there was a large expansion in the fraction of granule cells responsive to both auditory (13.1 ± 1.3%, $P<0.0001$, n = 26, paired t-test) and somatosensory (7.7 ± 2.1%, $P=0.0056$, n = 12, paired t-test) stimuli (Fig. 2a,b). Two points merit emphasis: First, these results indicate that the granule cell fluorescent responses we have measured are unlikely to reflect subthreshold activity, as the majority of granule cells were not responsive until inhibition was blocked. These cells necessarily received excitatory input in control conditions that was not reported by GCaMP activity. Second, the sparsity of granule cell population responses we have measured is due to local synaptic inhibition, and not due to a sparsity of incoming mossy fiber input.

Granule cell synaptic inhibition establishes discrete sensory ensembles via multiple computations

Given that each stimulus evokes sparse granule cell activity under control conditions, we next asked whether individual granule cells respond selectively to distinct stimuli. We find that granule cells prefer individual stimulus features, wherein cells that respond robustly to auditory stimuli of a given frequency respond only weakly to other frequencies (Fig. 2a,c; all comparisons: $p<0.0001$, one-way ANOVA). Similarly, neurons that respond to a given somatosensory (Fig. 2e; all comparisons: $p<0.0001$) or auditory (Supp. Fig. 8; all comparisons: $p<0.0001$) stimulus intensity respond weakly to other intensities. As such, populations of granule cells that respond to each stimulus feature establish discrete ensembles in response to these sensory inputs (Fig. 2i,k; auditory fraction overlap: 0.53 ± 0.02, n = 6; somatosensory: 0.06 ± 0.01, n = 3).

Notably, we observed less overlap in somatosensory ensembles than auditory ensembles. However, this was likely due to the smaller size of somatosensory ensembles. On average, auditory ensembles contained 83.7 ± 14.7 cells, (n = 18), whereas somatosensory ensembles contained only 29.4 ± 6.5 cells (n = 9). Therefore, the average overlap for auditory ensembles was 44.3 ± 0.2 cells, but only 1.8 ± 0.1 cells for somatosensory ensembles.

Despite representing different stimuli with discrete ensembles, there was significant variability across trials within each ensemble of cells responding to any given stimulus feature (Fig. 2 j,l). On average, each ensemble of responsive granule cells was only weakly correlated across trials (auditory: correlation coefficient (ρ) = 0.222 ± 0.004; somatosensory: ρ = 0.3454 ± 0.0774). Thus, while the sparse population response allows for discrete granule cell ensembles to represent individual stimulus features on average, the ensembles are surprisingly stochastic across trials, a feature that may contribute to the relatively slow time course of most cerebellar learning.

We next tested how GABAergic inhibition regulates stimulus preferences in granule cells. In neocortical cells, there is evidence that sensory tuning can by sharpened by local synaptic inhibition in some conditions[34]. For granule cells matched between control and after DART infusion (i.e. those responsive in both conditions), we find that removal of synaptic inhibition has a modest effect on stimulus preferences (Fig. 2b,d,f), as mean population preferences remained significant when inhibition was blocked (Supp. Fig. 9; auditory: all comparisons: $p<0.0001$; somatosensory: all comparisons: $p<0.0001$). While stimulus tuning was sharpened modestly by blocking inhibition, these data suggest that granule cell stimulus preferences are largely inherited from presynaptic mossy fiber input, consistent with the small number of mossy fibers that impinge on individual granule cells and the lack of recurrent processing among granule cells. However, considering all cells responsive in DART, which include a large number of cells that were unresponsive in control conditions, we find significantly more overlap between the ensembles that are responsive to each individual stimulus (Fig. 2i,k; auditory: 0.90 ± 0.02, n = 6, $P<0.0001$, unpaired t-test;; somatosensory: 0.16 ± 0.03, n = 3, $P=0.0266$, unpaired t-test). The large number of newly active cells in DART also added variability to ensemble identities, as ensembles became less correlated across trials when inhibition was blocked (Fig. 2 j,l; auditory: 0.116 ± 0.009, 21.9 ± 0.8 trials/ensemble, $P<0.0001$, unpaired t-test; somatosensory: 0.238 ± 0.065, 16.7 ± 2.9 trials/ensemble, $P=0.3455$, unpaired t-test). These results suggest that the higher mean response probability in DART (Fig. 1) is not sufficient to counter the variability introduced by the large number of additional responsive cells when inhibition is blocked. Together, these results indicate that inhibition serves to segregate granule cell ensembles representing discrete stimulus features largely by thresholding population activity.

Our data indicate that excitatory inputs from mossy fibers and local synaptic inhibition can establish unique ensembles of granule cells that encode individual sensory stimuli. However, it has also been demonstrated anatomically and physiologically that some granule cells receive mossy fiber input from more than one source[7-9], and it is thought that integration of these inputs can enhance the diversity of granule cell encoding[5-7]. Therefore, we next tested the principles that govern this integration by examining population responses to overlapping stimuli of two different modalities (Figure 3).

Consistent with previous single cell recordings showing enhanced spiking in response to convergent multimodal mossy fiber input[7, 9], we find that some cells exhibit larger responses to combined auditory and somatosensory input than to somatosensory input alone (Supp. Fig. 10, “facilitated”) (tone = 0.1 ± 0.3% ΔF/F, puff = 14.5 ± 1.2% ΔF/F, tone + puff = 28.3 ± 1.7% ΔF/F, n = 161, $P < 0.0001$, RM ANOVA, tone vs. puff: $P < 0.0001$, tone vs. tone + puff: $P < 0.0001$, puff vs. tone + puff: $P < 0.0001$, Tukey’s multiple comparisons test). Thus, part of the population code representing multisensory stimulus combinations is reflected by increased activity within the same cells that respond to each stimulus in isolation.

We also find, however, that the identity of cells that define multisensory ensembles differ with respect to the ensembles representing each stimulus in isolation in two important ways: First, we find that many granule cells with no significant responses to either stimulus alone became active in response to combined auditory and somatosensory stimulation (Figure 3a,b,g, “emergent”) (tone = 0.0 ± 0.1% ΔF/F, puff = 0.0 ± 0.1% ΔF/F, tone + puff = 7.6 ± 0.5% ΔF/F, n = 488, $P < 0.0001$, RM ANOVA, tone vs. puff: $P = 0.9996$, tone vs. tone + puff: $P < 0.0001$, puff vs. tone + puff: $P < 0.0001$, Tukey’s multiple comparisons test). These data suggest that integration of both

stimulus modalities is necessary to drive these granule cells above spike threshold. These 'emergent' cells thus generate a novel multisensory ensemble by adding new cells that are not present in the ensembles representing each stimulus in isolation.

Second, however, we also observed a large population of granule cells that are suppressed in response to combined somatosensory and auditory stimulation (Figure 3c,d,g, "suppressed") (tone = -0.1 ± 0.2% ΔF/F, puff = 13.7 ± 1.2% ΔF/F, tone + puff = 4.9 ± 0.8% ΔF/F, n = 355, P < 0.0001, RM ANOVA, tone vs. puff: $P < 0.0001$, tone vs. tone + puff: $P < 0.0001$, puff vs. tone + puff: $P < 0.0001$, Tukey's multiple comparisons test). Many of these cells are completely silenced, thus subtracting them from the ensembles representing individual stimuli in isolation. This effect therefore further separates the new, multisensory ensemble from the unisensory ensembles. Together, the emergent and suppressed populations of granule cells represent the vast majority of total granule cells in our measurements (Figure 3g). This suggests that whatever mechanism is responsible for these computations is critical for the encoding of complex multisensory stimuli in the granule cell layer.

To test whether local synaptic inhibition provides the necessary mechanism to establish these suppressed and emergent populations, we again utilized the DART system to acutely block inhibition. An analysis of matched cells between control and DART conditions revealed that inhibition powerfully shapes both the emergent and suppressed granule cell populations (Fig. 3 e,f,g). Specifically, though emergent cells had no significant response to either stimulus alone in control conditions, we find that blocking synaptic inhibition revealed responses to each individual stimulus (Fig. 3e)(tone = 0.8 ± 2.9% ΔF/F, puff = 2.1 ± 0.6% ΔF/F, tone + puff = 5.9 ± 0.5% ΔF/F), again consistent with a spike thresholding effect. These data also contextualize the strategy of utilizing widespread subthreshold input instead of sparse, high-fidelity suprathreshold input, as it would not be possible to generate these unique emergent multisensory ensembles with the latter strategy.

We also find that the suppressed population was dependent on synaptic inhibition, as suppression was abolished in the presence of DART (Fig. 3f) (tone = 1.5 ± 0.6% ΔF/F, puff = 10.7 ± 2.3% ΔF/F, tone + puff = 8.5 ± 1.8% ΔF/F, n = 43, $P < 0.0001$, RM ANOVA, tone vs. puff: $P = 0.0003$, tone vs. tone + puff: $P = 0.0003$, puff vs. tone + puff: $P = 0.3838$, Tukey's multiple comparisons test). These data indicate that inhibition can be recruited in a stimulus-specific manner, where in this case, auditory input can recruit inhibition that suppresses responses to somatosensory input. In this manner, local inhibition can mediate subtractive stimulus integration, operating to suppress the response of one input when another is present. Consistent with theoretical work, which has hypothesized that such a mechanism could act to diversify granule cell representations by reducing ensemble overlap during combined stimulus representations[35], our data indicate that stimulus-specific suppression provides a widespread and powerful means to generate unique multisensory ensembles.

To further explore this computation, we varied the features of co-presented stimuli (Fig. 3h,i,j). We find that suppression can be specific even within the same modality during co-presentation of stimuli with different features (Fig. 3h,i). These data reveal that local synaptic inhibition is a crucial source for generating diversity in granule cell population responses during complex sensory input, segregating multisensory ensembles from each other and from those representing each stimulus in isolation.

Granule cell sensory responses are temporally variable

In addition to population identity, the timing of granule cell activity has also been hypothesized to play an important role in behavior and learning[4]. Therefore, we also tested how granule cells represent the timing of sensory input and how this depends on local synaptic inhibition. We find that the average responses of individual granule cells during a 1 second auditory stimulus forms a population response that tiles the duration of the stimulus (Fig. 4a)[36]. Surprisingly, however, we find that granule cells do not respond with reproduceable timing across trials (Fig. 4a). Because the peak of mean $\Delta F/F$ responses can be biased by a small number of trials with large responses, we also computed response timing according to the onset of fluorescent responses during the stimulus window (Fig. 4b,c). This measure again supports the conclusion that granule cell responses are not reproduceable in their timing across trials (Fig. 4c). To quantify this variability, we measured the jitter in response onset across trials (Fig. 4d) and found that granule cells have an onset time that varies by hundreds of milliseconds across trials (Figure 4f; control onset S.D. = 0.7721 ± 0.0218). These results suggest that individual granule cells do not exhibit a high degree of across trial consistency, even for a relatively short 1 second stimulus, as has been thought necessary for cerebellar learning[37].

We find that blocking synaptic inhibition shifts the distribution of response onset times earlier (Figure 4e and Supp. Fig. 11-12; first peak: control = 391.2 ± 11.5 ms, DART = 235.6 ± 5.5 ms, n=478, $P<0.0001$, paired t-test). Surprisingly, however, we do not observe a corresponding reduction in response jitter (Figure 4f, DART onset S.D. = 0.7729 ± 0.0227, $P=0.59$, paired t-test). This was due to the higher response probability across trials in the DART condition, where there were many more total trials with significant stimulus responses (Fig 4d). As a result, while there were more trials with earlier response times when inhibition was blocked, there were also more trials with late responses, preventing an overall change in mean response jitter (Figure 4d,f). These data are consistent with previous results suggesting that response timing in granule cells is not exclusively regulated by synaptic inhibition[38] and must, therefore, also reflect parameters such as variability in input timing, and cellular properties such as short-term plasticity of mossy fiber input[7] and the intrinsic membrane properties of granule cells[39].

In control conditions, we also find that many granule cells respond at or near the offset of the auditory stimulus (Fig. 1c, 4a,g). These 'off' cells represented 5.4% of the responsive population. When inhibition was blocked, these cells responded much earlier during the auditory stimulus (Fig. 4g-h; n=47, $P<0.0001$, paired t-test). This indicates that under control conditions recruitment of inhibition during the sensory stimulus prevents these cells from responding, even though they receive sufficient excitation during the stimulus to drive spiking if inhibition is removed. Together, these data suggest that inhibition serves to diversify the temporal responses of granule cells by both limiting the number of early responses during a stimulus presentation and establishing a population of cells that selectively represents the termination of sensory input.

Granule cell synaptic inhibition is required for cerebellum-dependent sensory discrimination

Our data reveal that synaptic inhibition powerfully restricts the population of granule cells recruited by sensory input and shapes many features of the population ensembles that encode sensory stimuli. In principle, these effects are consistent with classical and recent computational models[5,

[6, 40] proposing that granule cell inhibition acts to segregate the population codes necessary for both learning and the expression of learned behaviors. To test this hypothesis directly, we utilized the cerebellum-dependent task delay eyelid conditioning. For this task, mice were trained on a freely moving treadmill[41] to associate a brief corneal air puff (unconditioned stimulus, "US") with a co-terminating neutral auditory tone (5 kHz, 250 ms; conditioned stimulus, "CS+"; Fig. 5a-d). We first trained mice until the probability of conditioned responses ("CR") in each session had plateaued (0.80 ± 0.06, n = 8; Fig. 5d). In a subset of mice, infusion of muscimol into the eyelid conditioning region of the cerebellar cortex at the floor of the primary fissure, which spread into the anterior interpositus[41], abolished conditioned responses, confirming cerebellar dependence (n = 3; Fig. 5c and Supp. Fig. 13).

To test whether mice could discriminate between the learned CS+ and similar auditory stimuli that had not been paired with a US during learning (CS-), we next measured responses in a cohort of mice for which two different CS- tones (1 and 10 kHz) and the CS+ tone were presented on randomly interleaved trials (Supp. Fig. 14). In these experiments, consistent with previous work in rabbits[42, 43], we find that the response probability and amplitude of CRs were significantly reduced for both CS- tones as compared to the CS+ tone (Supp. Figure 14; 1 kHz or 10 kHz, 250 ms; "CS-"; Figure 5; CR probability: CS+ = 0.76 ± 0.05, CS- (1 kHz) = 0.62 ± 0.04, CS- (10 kHz) = 0.49 ± 0.07, n = 4, P = 0.0034, RM ANOVA, CS+ vs. CS- (1 kHz): P = 0.0023, CS+ vs. CS- (10 kHz): P = 0.0019, Dunnett's multiple comparisons test; CR amplitude: CS+ = 0.42 ± 0.05, CS- (1 kHz) = 0.30 ± 0.02, CS- (10 kHz) = 0.28 ± 0.04, n = 4, P = 0.0103, RM ANOVA, CS+ vs. CS- (1 kHz): P = 0.0359, CS+ vs. CS- (10 kHz): P = 0.0049, Dunnett's multiple comparisons test).

To test whether granule cell inhibition is a critical component of sensory discrimination in this cerebellum-dependent task, we again utilized the DART system to block $GABA_A$Rs. In a well-trained cohort expressing HTP in granule cells in the eyeblink region of the cerebellar cortex (Fig. 5e), mice were subjected to 3 test sessions, each one week apart with daily CS+ only training in between (Fig. 5f). Test sessions with control infusions of saline or nbDART into the eyelid conditioning region revealed that trained mice effectively distinguished the CS+ from a single tone with a different frequency (10 kHz, 250 ms; "CS-") (Fig. 5g-h; saline, CR probability: CS+ = 0.80 ± 0.05, CS- = 0.48 ± 0.05, n = 5, P = 0.0036, paired t-test, CR amplitude: CS+ = 0.40 ± 0.04, CS- = 0.27 ± 0.04, n = 5, P = 0.0004, paired t-test, nbDART, CR probability: CS+ = 0.83 ± 0.05, CS- = 0.58 ± 0.07, n = 5, P = 0.0319, paired t-test, CR amplitude: CS+ = 0.43 ± 0.03, CS- = 0.35 ± 0.04, n = 5, P = 0.0314, paired t-test). However, blocking synaptic inhibition to granule cells in the eyelid conditioning region with functional DART reduced conditioned response probability and amplitude during CS+ trials such that behavior was indistinguishable from CS- trials (Fig. 5i; CR probability: CS+ = 0.56 ± 0.05, CS- = 0.50 ± 0.05, n = 5, P = 0.1894, paired t-test, CR amplitude: CS+ = 0.31 ± 0.03, CS- = 0.29 ± 0.02, n = 5, P = 0.2515, paired t-test). DART infusion did not significantly impact responses to the CS- (CR probability: saline = 0.48 ± 0.05, DART = X0.50 ± 0.05, P = 0.8928, paired t-test; CR amplitude: saline = 0.27 ± 0.04, DART = 0.29 ± 0.05, P = 0.6938, paired t-test). Interestingly, we did not observe an effect on the trajectory of CRs when granule cell inhibition was blocked (Supp. Fig. 15), suggesting that response kinematics may be largely shaped downstream, perhaps by inhibition and excitation onto Purkinje cells or elsewhere in the circuit. Together, these data indicate that granule cell inhibition is necessary for sensory discrimination in a cerebellum-dependent task and shapes the contextual representations that are harnessed for cerebellar behaviors.

Discussion

By imaging granule cell responses to discrete sensory input while manipulating local synaptic inhibition, we have revealed multiple key computations that extend classical Marr-Albus models of granule cell layer processing. First, we find that local synaptic inhibition enforces sparse granule cell population activity in terms of both response probability and cell number. Moreover, consistent with its role as a pattern separation layer, we find that granule cells represent sensory stimuli as discrete ensembles that also depend on inhibition to minimize overlap. For multisensory ensembles, inhibition plays a central role in defining population codes by establishing multisensory-only cells and by suppressing responses of unisensory ensembles in a stimulus-specific manner. In these ways, which were not envisioned by classical models, inhibition can generate novel multisensory granule cell ensembles. Finally, in agreement with our imaging data suggesting that inhibition serves a central role in pattern separation by establishing largely non-overlapping sensory representations, we find that granule cell inhibition is required for sensory discrimination in a cerebellum-dependent behavior.

Pattern Separation

Recent work has shown that, during complex behaviors, granule cell activity can be denser than was predicted by classical Marr-Albus models[15-18]. In contrast with these experiments, our goal was to isolate discrete sensory responses. In particular, our experimental design discarded trials with substantial animal movement, thereby revealing sparse population responses related to individual sensory representations. Additionally, we tested how specific representations depend on synaptic inhibition and, in doing so, isolated several novel mechanisms that enable pattern separation.

In our unisensory stimulus experiments, the role of inhibition in generating distinct stimulus representations was largely due to thresholding. Although the origins of auditory input to the cerebellum have not been exhaustively investigated, Crus I receives corticopontine inputs from the dorsal field of auditory cortex, as well as input from primary auditory cortex that is routed through subcortical nuclei and the inferior colliculus[23]. Given the tonotopic organization of primary auditory cortex, many mossy fibers likely relay frequency-tuned inputs that are then thresholded at the level of the granule cell, producing sparse representations that are generated by the subset of inputs capable of driving spiking.

Somatosensory information is transmitted to the cerebellar hemispheres through corticopontine inputs, as well as directly from the trigeminal nucleus [44], and can converge onto individual granule cells[45]. Granule cells have been reported to have small cutaneous receptive fields, with some cells receiving multiple somatosensory inputs[46]. In our experiments, the somatosensory airpuff may have reached multiple receptive fields. As such, the origins of the somatosensory amplitude preferences we have measured are unclear. However, previous work has described considerable diversity in the source and number of excitatory somatosensory inputs to individual granule cells that could influence stimulus preferences[45]. As with auditory stimuli, our data suggest that inhibition can shape stimulus preferences through thresholding, as blocking inhibition increased the responsive population, producing more overlap across ensembles.

Spike thresholding also plays a key role in generating unique multisensory ensembles by establishing cells that only respond to specific input combinations. For these cells, input from

each modality in isolation is insufficient to drive a response, but combined input during multisensory stimulation can overcome thresholding to generate a response. These multisensory-only cells rely on intact inhibition, as subthreshold inputs from individual stimuli become suprathreshold when inhibition is blocked. In this way, inhibition creates multisensory ensembles that are unique to specific stimulus combinations. Importantly, this mechanism of pattern separation would not be possible if sensory ensembles were instead established by sparse mossy fiber input that drove high fidelity granule cell spiking. Thus, we speculate that it may be more appropriate to consider thresholding inhibition as a mechanism to enhance combinatorial diversity of granule cell responses that to enforce population sparsity per se.

Beyond this broad thresholding effect, however, we also find that inhibition can be recruited in a stimulus-specific manner to provide subtractive refinement of granule cell population activity. This mechanism regulated the activity of a large fraction of cells in our multisensory experiments, representing a powerful additional means of pattern separation that has been previously uncharacterized in the cerebellum. Such stimulus-specific lateral inhibition was hinted at by early measurements suggesting that granule layer inhibition can vary according to the specific combination of vestibular afferent nerve stimulation[47], as well as by *in vitro* measurements suggesting that Golgi cells may be recruited in a pathway specific manner[48]. In addition, recent imaging experiments have revealed that, while many Golgi cells are synchronously active during behavior, a large fraction can also display diverse activity patterns that may suggest stimulus specific drive[49]. Here, our measurements reveal that stimulus-specific recruitment of inhibition is a widespread mechanism that shapes multisensory population activity *in vivo*. Notably, this mechanism is in direct opposition to the concept of Golgi cell inhibition of granule cells acting exclusively as a broad, general feedback system proposed by classical Marr-Albus theories. Thus, for multisensory inputs, the combination of adding new cells via thresholded summation and subtracting cells via stimulus specific inhibition provides a powerful means for pattern separation.

Together, these findings suggest that inhibition can provide the granule cell layer with an even greater capacity for pattern separation than was envisioned by classical Marr-Albus models, and it may serve to counteract the intrinsic limitations on combinatorial diversity that are imposed by the anatomical architecture of mossy fiber input to granule cells[50]. Moreover, these measurements support the idea that the granule cell layer can generate codes that are high dimensional[51], in particular by decorrelating sensory representations[52, 53]. Thus, even if granule cell activity exceeds the levels proposed in classical models during behaviors involving more diverse cerebellar input, these mechanisms may provide a basis for effective pattern separation.

Spatio-temporal variability of granule cell representations

Typically, models of cerebellar learning assume consistency of individual granule cell timing across trials, at least for stimulus durations that are appropriate for learning[37]. In contrast, however, our data show that granule cell responses occur with high temporal variability. The assumption that granule cell spike timing should be temporally reliable has previously been supported by measurements of subthreshold activity in granule cells in response to somatosensory input. These measurements have shown that timing of mossy fiber input can be highly reproduceable across trials[46]. Such measurements have not, however, revealed that consistency of mossy fiber input is translated into consistency of spike timing, which may vary

considerably due to intrinsic membrane properties and other inputs. For example, while our experiments are designed to address fast synaptic inhibition provided by $GABA_A$ receptors, they do not address the contributions of $GABA_B$ receptors[54], neuromodulators[38, 55], or cell-intrinsic conductances, such as voltage-activated potassium currents, that can alter the relationship between synaptic input and spiking[39]. We also note that the reliability of inputs may be modality specific[56], as different mossy fibers can have different strengths and short-term plasticity, and likely have different temporal consistency depending on source.

We also find that this variability was not dramatically altered when inhibition was blocked. In some circuits, feedforward inhibition can play a powerful role in establishing spike timing[57]. At the input layer of the cerebellum, however, slice recordings have suggested that feedforward recruitment of Golgi cell inhibition onto granule cells is relatively weak and variable across trials[58]. Moreover, *in vivo* recordings have demonstrated that stimulus evoked inhibitory postsynaptic currents onto granule cells often occur before the arrival of excitatory input[59] and, thus, may not enforce integration time windows. These experiments also suggest that granule cells are more likely to receive inhibition from Golgi cells activated by mossy fibers other than those providing direct excitation, or through feedback from the axons of other granule cells. Regardless, inhibition evoked before or during excitation likely serves primarily to increase granule cell spike thresholds[13, 60, 61], rather than as a timing mechanism, consistent with our current observations. As such, refinement of spike timing may not be a primary function of synaptic inhibition in the granule cell layer.

In addition to temporal variability, we observe considerable variability in the identity of granule cell ensembles representing sensory stimuli across trials, an effect primarily due to the relatively low probability of responses on single trials. This low response probability may provide part of the explanation for why cerebellar learning is slow to accumulate across trials, at least as compared to the requirements for induction of synaptic plasticity in the cerebellum when inputs are highly reproduceable[62].

Despite the spatio-temporal variability in granule cell representations we have measured, it is clear that the cerebellum can form learned associations that are both stimulus-specific and temporally precise[63]. While our measurements support mechanisms of pattern separation, most analogous learning circuits are also thought to involve a secondary process called pattern completion that stabilizes representations. Notably, our observations have been made in the absence of learning, and it remains possible that pattern completion processes in the cerebellar cortex serve to stabilize representations in space and time during learning. Indeed, the cerebellar cortex includes sites of plasticity at almost every node in the circuit, as well as a feedback pathway that provides the type of recurrent structure necessary for pattern completion circuits[64, 65]. Future measurements will be necessary to test how granule cell representations are altered across learning.

Granule cell inhibition and behavior

At the behavioral level, we have demonstrated that sensory discrimination is powerfully impaired in a cerebellum-dependent eyelid conditioning task when inhibition to granule cells is blocked. Specifically, we find that, when inhibition onto granule cells is blocked, conditioned responses to a CS+ and CS- become indistinguishable. If this change were simply due to mice equally

associating the CS+ and CS-, one might expect an increase in the probability of conditioned responses to the CS-. Instead, we observed only a decrease in the response probability to the CS+. This result is consistent with several observations from our imaging data.

First, granule cell tuning was largely preserved when inhibition was blocked, suggesting that the impairment of sensory discrimination is not specifically due to a shift in tuning of the 'learned' granule cell population. However, our data also show that blocking inhibition greatly increases the number of responsive cells (Figure 1). By definition, these emergent cells were not active during conditioning and, therefore, were not in the pathway of circuit modifications that occurred during learning (e.g., synapses onto Purkinje cells that may have been modified due to synaptic plasticity). With the emergence of these newly responsive cells, we find far greater overlap between granule cell populations that respond to different tones. Moreover, in line with previous experiments showing that blocking inhibition to granule cells significantly reduces the signal-to-noise ratio of sensory encoding[61], we find enhanced spontaneous activity when inhibition is blocked. For these reasons, we speculate that enhanced spontaneous activity and the emergent, unlearned CS+ responding cells combine to degrade the neural population response to the CS+, acting to bombard downstream Purkinje cells with non-specific signals that dilute those from the specific synapses modified during learning. Such results are consistent with a model whereby the cerebellum implements a probabilistic binary choice to recognize learned patterns[66], producing fewer CRs as the learned pattern becomes less discernable during acute block of granule cell inhibition.

Notably, our results partially differ from experiments in which large-scale lesions of the cerebellar cortex altered both the timing and probability of conditioned eyelid responses in rabbits[67]. The difference in outcome may suggest that the timing mechanism that controls the specific kinematics of the learned eyelid closure is mediated elsewhere in the cerebellar cortical circuit. Along with our observation that granule cell timing is largely inconsistent across trials, our results may suggest that the timing of eyelid responses is primarily computed downstream of granule cells, perhaps at the level of Purkinje cells, where inhibition from molecular layer interneurons directly sculpts the rate and timing of Purkinje cell spiking[68, 69].

Our data suggest that granule cell representations and behaviors associated with these patterns are highly dependent on inhibitory tone, consistent with findings that chronic hyperexcitability of granule cells can lead to diverse behavioral changes[70]. Because behavior and learning can be context-specific, we suggest that factors regulating granule cell inhibition may provide a powerful basis for enhancing patterns that should be learned or preventing learning in other contexts. In particular, Golgi cells can be bi-directionally modulated by acetylcholine and serotonin[38, 55]. Thus, our measurements suggest that these neuromodulators are likely candidates to enable context specific cerebellar behavior and learning. These neuromodulators could, for instance, enable the flexibility to express a CR in some contexts but not others.

Together, our results reveal several new mechanisms of cerebellar granule cell layer pattern separation that depend on local synaptic inhibition. These findings thus significantly extend long-standing predictions of classical Marr-Albus models for how the cerebellar cortex establishes and utilizes discrete sensory representations to guide behavior.

Methods:

Mice

All experimental procedures using animals were performed with approval of the Duke University Animal Care and Use Committee. Experiments were conducted during the light cycle with both male and female adult mice (>P60). All mice were housed with 12 h light/dark cycles with food and water ad libitum. Imaging experiments were performed with Ai148 (TIT2L-GC6f-ICL-tTA2)-D (Jackson Labs 030328) mice crossed with BACα6Cre-A[20] (n = 21). Eyelid conditioning experiments used BACα6Cre-A mice (n = 5).

Surgical procedures

Animals received dexamethasone (3 mg/kg) 3–4 h before surgery. All surgeries were performed under anesthesia, using an initial dose of ketamine/xylazine (50 mg/kg and 5 mg/kg) 5 min before, and 1.0-2.0% isoflurane throughout surgery. Breathing rate and toe pinch responsivity were continuously monitored during surgeries. A heating pad (TC-111 CWE) was used to maintain body temperature. For imaging and eyelid conditioning mice, titanium headplates (HE Parmer) were attached to the skull with Metabond (Parkell). Animals received buprenex (0.05 mg/kg) and cefazolin (50 mg/kg) twice daily for 2 d after surgeries.

For imaging experiments, adult mice (P50–60) were given a 3-mm diameter craniotomy over Crus I at approximately 3.0 mm lateral and 4.3 mm posterior to lambda. Crus I was injected (WPI UMP3) with 150 nl of either AAV7m8-X0117-CAG-DIO-[$^{+}$HTP-GGSGG$_8$-GPI-2A-dTomato]-WPRE-pA (HTP$_{GPI}$) (1 × 10^{12}; Duke Viral Vector Core) or AAV7m8-6360D-CAG-DIO-[^{dd}HTP-GGSGG$_8$-GPI-2A-dTomato]-WPRE-pA (^{dd}HTP) (1 × 10^{12}; Duke Viral Vector Core) at a rate of 30 nl/min and a depth of 350 µm at 2–3 sites. Glass windows consisting of two 3-mm coverslips bonded to a 5-mm coverslip (Warner Instruments No. 1) with index matched adhesive (Norland No. 1) were installed in the craniotomy using Metabond. Imaging mice receiving saline and drug infusions received a plastic cannula (Plastics One; C315GS/PK length 0.5 mm) positioned immediately rostral to the imaging window and attached with Metabond. All mice were given 8 weeks to allow viral expression, including 1–2 weeks of habituation to head restraint.

For eyelid conditioning experiments, adult mice (P50–60) were given 0.3-mm diameter craniotomies at approximately 1.8 mm lateral and 5.85 mm posterior to bregma. Three equidistant 80 nl injections of either AAV-DIO-$^{+}$HTP$_{GPI}$ (1 × 10^{12}) or AAV-DIO-^{dd}HTP$_{GPI}$ (1 × 10^{12}) were performed at a rate of 30 nl/min and a depth of 4.0 mm. Mice receiving saline and drug infusions were implanted with a plastic cannula (Plastics One; C315GS/PK length 3.0 mm) over the injection site that was secured with Metabond. A subset of wild type mice (*n* = 3) received cannulas but no virus injection at the same location. Mice were given 8 weeks to allow viral expression, including a minimum of 2 weeks for recovery before habituation to head restraints and training.

Calcium imaging

Two-photon imaging was performed with a resonant scanning microscope (Neurolabware) using a 16X water immersion objective (Nikon CFI175 LWD 16xW 0.8NA). A polymer (MakingCosmetics, 0.4% Carbomer 940) was used to stabilize the immersion solution during imaging. For GCaMP and TdTomato imaging, a Ti:Sapphire laser tuned to 920 nm (Spectra Physics, Mai Tai eHP DeepSee) was raster scanned via a resonant galvanometer (8 kHz,

Cambridge Technology) onto the cerebellum at a frame rate of 30 Hz and a field of view of 278 µm × 117 µm (796 × 264 pixels) (Supp. Video 1). Scanbox software (Neurolabware) was used to collect data through a green filter (510 ± 42 nm band filter (SEMrock)) onto GaAsP photomultipliers (H10770B-40, Hamamatsu).

Behavior

During imaging, animals were head-fixed in a custom sled atop a piezoelectric sensor (C.B. Gitty, 41 mm 'jumbo' piezo) read from and triggered through a multifunction data acquisition device (90 Hz, USB X, National Instruments) to measure animal movement[30, 31]. In a subset of experiments, whole-body motion was simultaneously recorded from a CMOS camera (60 Hz, Genie Nano M640 NIR, Teledyne Dalsa) with a fixed focal length lens (6 mm f/2.8, Edmund optics). During imaging, frame-by-frame whisker and facial movements were monitored with the aid of IR LEDs (Swann) from a CMOS camera (60 Hz, Genie Nano M640 NIR, Teledyne Dalsa) with a fixed focal length lens (6 mm f/2.8, Edmund optics) positioned 13 cm above the animal's head. Piezoelectric and video data were acquired and aligned to imaging data using Scanbox software (Neurolabware) and custom code written in MATLAB (Mathworks). For imaging experiments, sensory stimuli were delivered in pseudorandomized 167 s blocks with randomized inter-trial intervals (ITI) using Mworks (http://mworks-project.org) and custom software written in MATLAB. For somatosensory stimulation, low intensity air puffs (10, 15, or 20 psi, a range of intensities found to produce little or no behavioral response, delivered block-wise) were delivered from a metal tube 5 cm from the center of the vibrissae (5630–10200 ms ITI; 18–29 trials/block). Pure tones of either 68 or 75 dB with frequencies of 1, 5, or 10 kHz were delivered individually block-wise or in randomized pairs for single auditory stimulation (3800–15000 ms ITI; 9–23 trials/block). Imaging sessions lasted between 1.25–2.25 hours.

For eyelid conditioning, the behavioral setup was constructed according to Heiney et al. (2014). Prior to experiments, all mice were habituated to head restraint on the same wheel used for training for 30–60 min/day until they calmly entered head restraints and walked comfortably on the wheel (5–10 d). Stimulus delivery and frame acquisition for video monitoring were triggered with an Arduino Uno microcontroller board (Arduino) controlled with modified Arduino and Matlab code written for Neuroblinks software (Medina lab). Mice were trained during daily sessions of 100–300 trials in which a 50-ms air puff (30 psi) was delivered 3 mm from the mouse's cornea (unconditioned stimulus, US) and paired with a co-terminating 250-ms, 5 kHz, 70 dB tone (conditioned stimulus, CS). Each session contained one randomly delivered CS only test trial and one US only test trial. Trials were only initiated if the eyelid was open >70–80% for at least 200 ms and at a minimum of 10 s apart[41].

In vivo pharmacological infusions

Saline and drugs were infused into awake, head-fixed mice using an automated pump (WPI UMP3), a Hamilton syringe (10 µl Gastight model 1701 RN) and a plastic internal cannula (Plastics One, C315IS) threaded into the guide cannula. All infusions had a total volume of 1 µl delivered at a rate of 1 µl/min. To estimate the spread of pharmacological agents under the imaging window, 10 mM fluorescein dye (Sigma-Aldrich #F6377) dissolved in sterile artificial cerebrospinal fluid (aCSF; 150 nM NaCl, 4 mM KCl, 2 mM MgCl2, 2 mM CaCl2, 10 mM HEPES, 10 mM glucose, pH 7.4) was infused through the cannula rostral to the imaging window, followed by a 1 h rest and perfusion. For all other imaging and behavior experiments, aCSF only or either 1 µM non-binding gabazine.1^{nbDART} or 1 µM gabazine.1$^{nbDART.2}$ was dissolved in sterile aCSF and

applied, followed by a 20-min rest. Infusions were delivered at least 1 d apart for each animal. At least one day after gabazine.1^{nbDART} administration, 1 μM Alexa647.1$^{DART.2}$ was dissolved in sterile aCSF and infused, followed by 1 h rest and perfusion. In a subset of eyelid conditioning experiments, fluorescent muscimol (1 mM; BODIPY TMR-X muscimol conjugate; Invitrogen) was infused in wild type mice, followed by a 3-min rest period.

Histology

Mice were anaesthetized with an IP injection of ketamine/xylazine (200 mg/kg and 30 mg/kg, respectively) prior to perfusion with PBS and 4% paraformaldehyde. 50 μm sagittal sections were cut using a vibrotome (Pelco 102). Slices were mounted using Southern Biotech DAPI-Fluoromount G or Vectashield Vibrance (Vector labs) then imaged using an upright confocal microscope (Leica SP8).

Data Analysis

Multi-photon imaging: All acquired two-photon images were processed using a combination of the opensource Python toolbox for large scale calcium imaging data analysis CaImAn[71] and custom code written in MATLAB. First, images were corrected for motion over 60 × 60-pixel patches using a piecewise rigid motion correction algorithm (NoRMCorre;[72]). All videos were manually screened to ensure adequate motion correction. Whole experiments that could not be made to produce a stable averaged image were excluded from further analysis. Images collected before and after drug infusions, without displacing the objective, were motion registered and segmented together to enable reliable comparison between conditions. Then, source separation was performed using constrained non-negative matrix factorization (CNMF; [73]). This algorithm includes exclusion of fluorescence changes originating in the neuropil. Regions of interest (ROI) identified by CNMF were then sorted according to spatial stability, transient signal-to-noise ratio, and performance in a CNN based classifier[71]. ROIs were then excluded based on their proximity to the edge of the FOV and overlap with non-specifically-labelled structures (i.e., anything other than putative granule cells) in motion-registered, averaged images using custom MATLAB code. Remaining raw Ca2+ time courses computed by CNMF were screened for periods in which the signal exceeded 6 standard deviations from the mean of either the first or last 20,000 imaging frames for >2 s, as such changes were noted to occur in cells that become bright and swell over the course of an experiment and were presumed to be unhealthy/dying. ROIs with this fluorescence signature and a bright, swollen appearance in motion-registered, averaged images were excluded from further analysis. Additionally, raw Ca2+ time courses lacking stability by 1) slowly drifting in magnitude or 2) transiently or permanently losing all signal were excluded from further analysis to allow reliable comparison of responses throughout each experiment. Fluorescence changes (ΔF) were normalized to a 1-s window of baseline fluorescence prior to stimulus onset for each trial. Individual cell responses were considered significant if they surpassed 2 standard deviations from the baseline period between 90–180 ms after stimulus onset (somatosensory stimulation), or if any sliding window beginning at stimulus onset and ending 90 s after stimulus offset surpassed 2 standard deviations of any equal-length window during the baseline period (auditory stimulation). Some cells with significant responses in the control condition no longer achieved significance after DART infusions due to high levels of activity in the baseline period, despite having activity during the stimulus windows. Because this reduced signal-to-noise impaired accurate measurement of sensory responses, cells that lost significance in DART were not included for condition-matched analyses. The fraction of responsive granule cells for each condition was estimated by calculating the number of granule

cell sized ROIs (~14.7 pixel diameter) that would tile the FOV (796 x 264 pixels) without overlap. First and peak event times and amplitudes during individual trials were calculated using trapezoidal numerical integration, identifying peaks ≥120 ms. 'Off' cells were defined as cells having a mean first peak time at or after stimulus offset.

Behavior: For imaging experiments, a machine-learning-based algorithm (DeepLabCut[74]) was used to automatically track components of the face, whiskers, and head in accompanying high-speed videos. Tracked features were initially labeled manually in a small portion of frames (30) to train the algorithm, then x and y locations of each feature were automatically determined for all remaining frames. Motion was evaluated as cumulative displacement of these coordinates during aligned calcium imaging frames.

To validate the effectiveness of the piezo sensor at detecting motion, the same sensory stimuli used in imaging experiments were delivered while collecting high-speed video of each mouse's head and limbs. Machine learning-based motion tracking with DeepLabCut[29] revealed that the sensor reliably detects limb motion and other movements such as grooming (Supp. Fig 5). Specifically, limb and facial movements were aligned with piezo traces, revealing that piezo measurements reliably reflect movements of all four limbs, as well as fine movements of the ears and face. Video detected motion and piezo recordings do not have a one-to-one relationship, however, and some changes in piezo voltage do not correspond with any visible movement detected by video. We interpret these changes in piezo voltage as likely to reflect muscle tension as the mouse prepares to move, as they generally occur immediately preceding video detected movements. However, nearly all video-detected movements are less than 5 frames away from piezo deflections that are >1 standard deviation from the mean, so this threshold was used to segregate imaging frames recording during movement. Trials were excluded from analysis if movement occurred anytime between the second before stimulus onset and 300 ms after stimulus offset.

In addition to removing signals related to movement, piezo voltage traces identify frames in which significant animal movement causes failures of imaging motion correction. Two-color imaging of both neural activity with GCaMP6f and tdTomato indicates that instances of tdTomato fluorescence fluctuations (indicating Z-motion or another motion correction failure) are also excluded from analysis using the above criteria (Supp. Fig 5).

Because mice whisk frequently, and granule cells in Crus I can be tuned to whisker movements[24, 26] , we used a different approach to segregate cells that are modulated during whisking. During imaging, videos of the head and whiskers were used to align whisker movements to changes in granule cell activity. Because some granule cells can be tuned for whisker deflection angle[24], whisker movements were then parsed according to movement amplitude, and whisks that occurred between trials and in the absence of whole-body movement were used to identify granule cells that were modulated specifically by whisking. Whisk modulated cells overlapped very modestly with ensembles responsive to auditory or somatosensory stimulation (7.7 ± 4.5% of sensory and whisking responsive cells). Accordingly, inclusion of whisk modulated cells had no significant effect on auditory (unpaired t-test, P=9686) and somatosensory (unpaired t-test, P=4864) responses on average. (Supp. Fig 4).

For eyelid conditioning experiments, behavioral data were analyzed using modified Matlab code written for Neuroblinks software (Medina lab). Briefly, fraction of eyelid closure was calculated for each video frame by generating a binary image of a region of interest surrounding the eye, thresholded to provide maximal discriminability for each experiment, then summing pixel counts for each frame. Conditioned responses (CRs) were defined by eyelid closure >10%. CR probability for a given session was calculated according to all paired trials during that session. CR amplitudes were calculated as the mean closure during a 4-frame window preceding the US.

Figure Legends

Figure 1. Local synaptic inhibition sparsens and thresholds cerebellar granule cell sensory responses. a. Schematic of experimental approach. **b.** Example average field of view across trials of granule cells expressing GCaMP6f during presentation of a somatosensory stimulus in the absence of whole-body movement. Yellow arrows designate significantly responsive cells. **c.** Top, example calcium traces (ΔF/F) from a granule cell on sequential tone presentation trials before (black) and after (red) gabazine.1$^{DART.2}$ infusion ("DART", 1 μM). Bottom, mean responses of all cells with significant responses to a tone before (left) and after DART application (right) in an example mouse with granule cell HTP expression. Example cell above is cell 46. **d.** Mean time course of responses during tone presentation before (black) and after (red) DART infusion. Error is SEM across cells (n=3360 cells). **e.** Mean response amplitudes for individual cells before (black) and after (red) DART infusion. Black lines are mean ± SEM across cells. **f.** Same as **e**, for response probability. **g.** Same as **e**, for mean responses on all trials with significant responses (n=1942). **h-l.** Same as **c-g,** for responses to somatosensory stimuli (i-k, n=815 cells, l, n=118 cells). Example cell in **h** is cell 192 in the heatmap. ****p < 0.0001.

Figure 2. Cerebellar granule cells have stimulus feature preferences that are largely independent of local synaptic inhibition. a. Number of responsive cells in each experiment (colors) and across all experiments (black) before and after DART for auditory (left) and somatosensory (right) stimuli. Colors represent specific stimulus conditions; error is SEM across conditions. **b.** Same as **a**, for fraction of total responsive cells. **c.** Normalized responses in control conditions for all granule cells responsive to 68 dB tones, grouped according to the frequency that drove the maximum response: 1 kHz: n = 227 cells; 3 mice; 5 kHz: n = 211 cells; 10 kHz: n = 166 cells. Error is SEM across cells. **d.** Same as **c**, for tone-responsive granule cells before and after DART infusion (red; 1 kHz: n = 250 cells, 5 kHz: n = 297 cells, 10 kHz: n = 169 cells). **e.** Same as **c**, for granule cells responsive to 72 dB tones preferring: 1 kHz: n = 184 cells; 5 kHz: n = 141 cells; 10 kHz: n = 313 cells. **f.** Same as **d**, for tone-responsive granule cells before and after DART infusion (red; 1 kHz: n = 170 cells, 5 kHz: n = 331 cells, 10 kHz: n = 224 cells). **g.** Same as **c**, for all puff responsive cells preferring: 10 PSI: n = 45 cells; 3 mice; 15 PSI: n = 47 cells; 20 PSI: n = 74 cells. **h.** Same as **d**, for puff responsive cells before and after DART infusion (red; 10 PSI: n = 100 cells, 15 PSI: n = 69 cells, 20 PSI: n = 202 cells). **i.** Fraction of overlap for each stimulus condition (colors) and across all conditions (black) before and after DART for auditory (left) and

somatosensory (right) stimuli. Error is SEM across conditions. **j.** Same as **i** for the Pearson's correlation of neuronal identity across trials.

Figure 3. Coincident stimuli create unique granule cell ensembles. a. Time course of responses to uni- (tone: gray; puff: blue) and multisensory (tone + puff: green) stimuli for an example emergent cell. Error is SEM across trials. **b.** Left, same as **a**, for all emergent cells (n=79, subset matched to DART condition). Right, amplitude of responses to tone, puff and tone + puff for all matched emergent cells. Error is SEM across cells. **c-d.** Same as **a-b**, for matched suppressed cells (n=43). **e-f.** Same as **b** and **d**, for matched cells after DART infusion. **g.** Pie charts illustrating relative prevalence of each response category before (top; facilitated: n=161, unchanged: n=158, suppressed: n=355, emergent: n=488) and after (bottom; facilitated: n=172, unchanged: n=93, suppressed: n=63, emergent: 676) DART infusion. **h-i.** Example cells illustrating stimulus-specific suppression. Both cells respond robustly to the puff alone (blue), but each is suppressed in response to a specific combination of puff and tone of a given frequency and amplitude (dark green), but not a different frequency and amplitude (light green). Error is SEM across trials. **j.** Granule cell layer circuit motif that would produce emergent responses (left) and stimulus-specific suppression (right). GrC- granule cell; GoC- Golgi cell. ***$p < 0.001$, ****$p < 0.0001$.

Figure 4. Cerebellar granule cells respond with temporal variability to auditory stimuli. a. Left, mean tone-evoked responses on the first half of trials for all cells ordered by peak response time (n = 478 cells). Right, same as on left for the second half of trials, ordered according to peak responses during the first half. **b.** Example calcium traces ($\Delta F/F$) from a granule cell during sequential tone presentation trials. Arrow notes first event following tone onset. **c.** Left, heatmaps displaying the mean first event time probabilities for all cells during the first half of trials ordered by timing of greatest first event probability. Right, first event time probabilities during the second half of trials ordered the same as on left. **d.** Heatmaps displaying peak event times for all significant trials for an example cell in control (top) and after DART infusion (bottom). **e.** Cumulative distribution of mean first event times for all cells in control (black; n=1631) and after DART infusion (red; n=3718; Kolmogorov-Smirnov $P<0.0001$). **f.** Same as **e**, for mean standard deviation of first event times (Kolmogorov-Smirnov $P=0.9859$). **G.** Example traces in control (black) and after DART infusion (red) for two example cells. Note the cell on the top has an increase in peak activity without a change in onset, while the cell on the bottom responds to tone offset in control but tone onset in DART. **H.** Mean response time in control (black) and after DART (red) for cells with a mean first peak time at or after tone offset in control conditions (n=47; paired t-test $P<0.0001$).

Figure 5. Local synaptic inhibition is necessary for expression of a sensorimotor association. a. Schematic of experimental design. CS- conditioned stimulus (tone); US- unconditioned stimulus (corneal air puff). **b.** Sample frames before (top) and after (bottom) air puff delivery. Blue oval indicates ROI analyzed to evaluate conditioned responses. Insets show thresholded binary image used for calculating fractional eyelid closure. **c**. Top, example consecutive eyelid traces from a trained mouse. Blue line mark onset of tone (CS). Red line marks onset of US. Note the eyelid begins to close before the US. Bottom, time course of

conditioned response (CR) amplitude for a trained mouse on trials before and after local infusion of muscimol (1 mM). **d.** Average CR probability (top) and amplitude (bottom) during training (n=8 mice). Error is SEM across mice. **e.** Example confocal images (scale 50 µm) of a representative mouse expressing HTP (red) in granule cells in the eyelid conditioning region with bound Alexa647.1$^{DART.2}$ (cyan). Top, pl: posterior lobe; al: anterior lobe; pf: primary fissure. Bottom, ml: molecular layer; gc; granule cell layer. **f.** Experimental time course. CS+: tone frequency paired with air puff (5 kHz); CS-: unpaired tone frequency (10 kHz); nbDART: non-binding gabazine.1^{nbDART}. **g.** Average CR probability (top) and amplitude (bottom) for individual mice during presentation of CS+ and CS- trials after saline infusion (n=5 mice). **h.** Same as **g**, after infusion of gabazine.1^{nbDART} (1 µM). **i.** Same as **g**, after infusion of gabazine.1$^{DART.2}$ (1 µM). *p < 0.05, **p < 0.01 ***p < 0.001.

Supplemental Figure 1. Selective labeling of cerebellar granule cells. a. Example confocal images from a representative mouse expressing GCaMP6f (left) and HTP (middle) and their intersection (right) in the granule cell layer (GcL). Arrows note sparse labeling of Purkinje cells, which were excluded from analysis. **b.** Same as **a**, for a different representative mouse infused with Alexa647.1$^{DART.2}$ (cyan, middle right) and intersection of all three labels (right).

Supplemental Figure 2. Local synaptic inhibition sparsens and thresholds cerebellar granule cell responses to all auditory stimuli presented. a. Top left, mean time course of responses during 1 kHz, 68 dB tone presentation before (black) and after (red) DART infusion. Error is SEM across cells. Top right, mean response amplitudes for individual cells before (black) and after (red) DART infusion. Black lines are mean ± SEM across cells. Bottom left, same as top right, for response probability. Bottom right, same as top right, for mean responses on all trials with significant responses (n=689 cells, n=458 cells for single values; 6 mice). **b.** Same as **a**, for 1 kHz, 72 dB tones (n=541, n=296 for single trial values; 5 mice). **c.** Same as **a**, for 5 kHz, 68 dB tones (n=381; n=184 for single trial values; 3 mice. **d.** Same as **a**, for 5 kHz, 72 dB tones (n=493cells, n=251 for single trial values; 3 mice). **e.** Same as **a**, for 10 kHz, 68 dB tones (n=638 cells, n=409 cells for single trial values; n=6 mice). **f.** Same as **a**, for 10 kHz, 72 dB tones (n=566; n=292 for single trial values; 3 mice). *p < 0.05, ****p < 0.0001.

Supplemental Figure 3. Local synaptic inhibition sparsens and thresholds cerebellar granule cell responses to all somatosensory stimuli presented. a. Top left, mean time course of responses to a 10 PSI air puff before (black) and after (red) DART infusion. Error is SEM across cells. Top right, mean response amplitudes for individual cells before (black) and after (red) DART infusion. Black lines are mean ± SEM across cells. Bottom left, same as top right for response probability. Bottom right, same as top right for mean responses on all trials with significant responses (n=283 cells; n=58 cells for single trial values; 6 mice). **b.** Same as **a**, for 20 PSI air puff (n=234, n=28 for single trial values; 3 mice). **c.** Same as **a**, for 30 PSI air puff (n=261, n=32 for single trial values; 3 mice).

Supplemental Figure 4. Tracking of whisker movements with high-speed video during imaging enabled identification of whisking modulated cells and evaluation of their contribution to sensory responses. a. Left, example image from a representative mouse with

features labeled for automated identification of two whisker root (light blue and red) and midpoints (orange and green), as well as a stationary feature (snout, dark blue) used to estimate tracking jitter. Right, image from **a** with x and y coordinates for anterior whisker midpoint for all frames overlaid. **b.** Time course of displacement (in pixels) of whisker midpoint labeled in **a**. Dashed lines indicate thresholds used to segregate whisks according to magnitude. **c.** Left, mean ± SEM of low amplitude whisks occurring between trials and in the absence of body movement during an example experiment (n = 816 whisks). Mean ± SEM of frames without whisker movement plotted behind. Right, same for high amplitude whisks measured during the same experiment (n = 287 whisks). **d.** Left, mean ± SEM fluorescence of cells modulated during small whisks and fluorescence of the same cells during frames without movement (n = 16). Right, same for independently identified cells modulated during large whisks (n = 16). Cells had the same identity. **e.** Fraction of responsive cells from 4 mice with significant activity during whisking, a sensory stimulus (auditory or somatosensory), or both; RM ANOVA: p = 0.0013, Tukey's multiple comparison's test: stim v. whisk: p=0.0025, stim v. w+s: p = 0.0036, whisk v. w+s: *P* = 0.5782). **f.** Top, Time course of mean responses to a somatosensory stimulus for all cells significantly responsive to the stimulus (orange; n = 366) and cells significantly responsive to the stimulus not modulated during whisking (black; n = 306; paired t-test of mean during stimulus window: control = 0.0343 ± 0.0066, DART = 0.0278 ± 0.0065, *P* = 0.4864). Error is SEM. Bottom, same as top for cells significantly responsive to an auditory stimulus (orange: n = 432; black: n = 424; paired t-test of mean during stimulus window: control = 0.0123 ± 0.0015, DART = 0.0122 ± 0.0014, *P* = 0.9686).

Supplemental Figure 5. Piezo vibration sensor reports body movements and facilitates removal of trials with z-motion. a. Example image from a representative mouse following automated identification of left (green) and right (orange) paws, nose (dark blue) and mouth (light blue). **b.** Time course of displacement (in pixels) of left paw and nose (top), right paw and nose (middle) during left paw lift (left) and grooming (right). Bottom, simultaneous motion measurement using a piezoelectric sensor under the mouse's torso. Shaded gray regions reflect motions greater than 1 standard deviation that were discarded. **c.** Example raw piezo sensor trace at low (top) and high (bottom) temporal resolution. Dashes at top of each trace indicate times of auditory or somatosensory stimulus presentation; dashed line indicates 1 standard deviation threshold. Shaded regions indicate epochs that exceed this threshold; red x indicates trial that was discarded. **d.** Example field of view with GCaMP6f (top) and tdTomato (bottom) expression. **e.** Time course of changes in fluorescence in the tdTomato channel (top) after x-y motion correction and fluctuations in the piezo sensor. Note that changes in tdTomato fluorescence correspond with periods of animal movement (arrowheads), likely corresponding to uncorrected effects of z-motion. **f.** Quantification of the mean number of tdTomato events detected during blocks in which the mouse was stationary or moving (n = 44 blocks; paired t-test P = 0.00177). Error is SEM across blocks.

Supplemental Figure 6. Probability and average amplitudes of auditory and somatosensory responses not changed after infusion of gabazine.1^{nbDART} variant. a. Heatmap of average responses to auditory stimuli in control conditions (left) and after infusion of **gabazine.1^{nbDART}** (nbDART, right) in an example mouse with HTP expression. **b.** Top left, mean

time course of responses during tone presentation before (black) and after (orange) nbDART infusion. Error is SEM across cells. Top right, mean response amplitudes for individual cells before (black) and after (orange) nbDART infusion. Black lines are mean ± SEM across cells. Bottom left, same as top right, for response probability. Bottom right, same as top right, for mean responses on all trials with significant responses (n = 2044, n = 1114 for single trial values; 3 mice). **c-d.** Same as **a-b**, for responses to somatosensory air puffs (n = 770, n = 259 for single trial values; 3 mice). *$p < 0.05$, ****$p < 0.0001$.

Supplemental Figure 7. Probability and average amplitudes of auditory and somatosensory responses not changed after infusion of DART with expressed non-binding ^{dd}HTP. a. Heatmap of average responses to auditory stimuli in control conditions (left) and after infusion of DART (right) in an example mouse with ^{dd}HTP expression. **b.** Top left, mean time course of responses during tone presentation before (black) and after (red) DART infusion. Error is SEM across cells. Top right, mean response amplitudes for individual cells before (black) and after (red) DART infusion. Black lines are mean ± SEM across cells. Bottom left, same as top right, for response probability. Bottom right, same as top right, for mean responses on all trials with significant responses (n = 1853, n = 1723 for single trial values; 2 mice). **c-d.** Same as **a-b**, for responses to somatosensory air puffs (n = 443, n = 266 for single trial values; 2 mice). *$p < 0.05$, **$p < 0.01$, ****$p < 0.0001$.

Supplemental Figure 8. Granule cells display preferences for auditory stimulus amplitude. a. Normalized responses for cells that prefer 68 dB (cyan; n = 342) or 72 dB (purple; n = 207) in response to 1 kHz tones. Error is SEM across cells. **b.** Normalized responses for cells that prefer 68 dB (left) or 72 dB (right) in control (cyan/purple) and after DART infusion (red; 68 dB: n = 390), 72 dB: n = 323). Data is the same as in **a** for control conditions. **c-d.** Same as **a-b**, for 5 kHz tones: control, 68 dB: n = 293, 72 dB: n = 213; DART, 68 dB: n = 220, 72 dB: n = 469 **e-f.** Same as **a-b**, for 10 kHz tones: control, 68 dB: n = 241, 72 dB: n = 367; DART, 68 dB: n = 381, 72 dB: n = 344.

Supplemental Figure 9. Granule cells display preferences for auditory stimulus frequency and amplitude and somatosensory stimulus amplitude before and after blocking synaptic inhibition. a. Left, maximum responses (ΔF/F) for cells significantly responsive to any 68 dB tones that prefer 1 kHz in control (n = 227) and DART (n = 250) conditions. Middle, same as left for cells that prefer 5 kHz: control: n = 211; DART: n = 297. Right, same as left for cells that prefer 10 kHz: control: n = 166; DART: n = 169. **b.** Same as a for cells significantly responsive to any 72 dB tones: 1 kHz, control: n = 184, DART: n = 170; 5 kHz, control: n = 141, DART = 331; 10 kHz, control: n = 313, DART: n = 224). **c.** Left, maximum responses (ΔF/F) for cells significantly responsive to 1 kHz at any amplitude that prefer 68 dB in control (n = 342) and DART (n = 207) conditions. Middle, same as left for cells responsive to 5 kHz that prefer 68 dB in control (n = 293) and DART (n = 220) conditions. Right, same as left for cells responsive to 10 kHz that prefer 68 dB in control (n = 241) and DART (n = 381) conditions. **d.** Same as c for cells that prefer 72 dB: 1 kHz, control: n = 207, DART: n = 323; 5 kHz, control: n = 213, DART: n = 469; 10 kHz, control: n = 367, DART: n = 344. **e.** Left, maximum responses (ΔF/F) for somatosensory stimulus responsive cells that prefer 10 PSI in control (n = 45) and DART (n = 100) conditions. Middle,

same as left for cells that prefer 15 PSI: control: n = 47, DART: n = 69. Right, same as left for cells that prefer 20 PSI: control: n = 74), DART: n = 202.

(auditory: 68 dB, 1 kHz preferring: 1 kHz = 5.2 ± 0.5% ΔF/F, 5 kHz = 2.0 ± 0.4% ΔF/F, 10 kHz = 1.8 ± 0.3% ΔF/F, n = 227, $P < 0.0001$; 5 kHz preferring: 1 kHz = 5.3 ± 0.6% ΔF/F, 5 kHz = 9.9 ± 0.8% ΔF/F, 10 kHz = 4.0 ± 0.4% ΔF/F, n = 211, $P < 0.0001$; 10 kHz preferring: 1 kHz = 2.4 ± 0.3% ΔF/F, 5 kHz = 2.2 ± 0.3% ΔF/F, 10 kHz = 5.4 ± 4.2% ΔF/F, n = 166, $P < 0.0001$; 72 dB, 1 kHz preferring: 1 kHz = 6.7 ± 0.5% ΔF/F, 5 kHz = 3.3 ± 0.4% ΔF/F, 10 kHz = 2.1 ± 0.2% ΔF/F, n = 184, $P < 0.0001$; 5 kHz preferring: 1 kHz = 3.4 ± 0.4% ΔF/F, 5 kHz = 6.0 ± 0.5% ΔF/F, 10 kHz = 1.6 ± 0.2% ΔF/F, n = 141, $P < 0.0001$; 10 kHz preferring: 1 kHz = 1.4 ± 0.2% ΔF/F, 5 kHz = 1.9 ± 0.2% ΔF/F, 10 kHz = 9.5 ± 0.4% ΔF/F, n = 313, $P < 0.0001$, RM ANOVA; 1 kHz, 68 dB preferring: low = 6.2 ± 0.5% ΔF/F, high = 2.7 ± 0.3% ΔF/F, n = 342, $P < 0.0001$; 72 dB preferring: low = 2.8 ± 0.2% ΔF/F, high = 5.9 ± 0.4% ΔF/F, n = 207, $P < 0.0001$; 5 kHz, 68 dB preferring: low = 8.7 ± 0.7% ΔF/F, high = 3.9 ± 0.6% ΔF/F, n = 293, $P < 0.0001$; 72 dB preferring: low = 1.8 ± 0.3% ΔF/F, high = 4.1 ± 0.3% ΔF/F, n = 213, $P < 0.0001$; 10 kHz, 68 dB preferring: low = 6.2 ± 0.4% ΔF/F, high = 1.9 ± 0.2% ΔF/F, n = 241, $P < 0.0001$; 72 dB preferring: low = 1.8 ± 0.2% ΔF/F, high = 8.6 ± 0.4% ΔF/F, n = 367, $P < 0.0001$, paired, two-tailed t-test; somatosensory: 10 PSI preferring: 10 PSI = 8.3 ± 3.1% ΔF/F, 15 PSI = 2.9 ± 1.3% ΔF/F, 20 PSI = 4.8 ± 2.8% ΔF/F, n = 45, $P < 0.0001$; 15 PSI preferring: 10 PSI = 1.3 ± 0.5% ΔF/F, 15 PSI = 4.0 ± 0.6% ΔF/F, 20 PSI = 0.7 ± 0.5% ΔF/F, n = 47, $P < 0.0001$; 20 PSI preferring: 10 PSI = 12.5 ± 3.1% ΔF/F, 15 PSI = 9.6 ± 2.3% ΔF/F, 20 PSI = 22.9 ± 4.0% ΔF/F, n = 74, $P < 0.0001$, RM one-ANOVA).

(DART: auditory: 68 dB, 1 kHz preferring: 1 kHz = 16.3 ± 0.7% ΔF/F, 5 kHz = 9.4 ± 0.4% ΔF/F, 10 kHz = 13.1 ± 0.6% ΔF/F, n = 250, P < 0.0001; 5 kHz preferring: 1 kHz = 8.7 ± 0.3% ΔF/F, 5 kHz = 15.1 ± 0.5% ΔF/F, 10 kHz = 8.7 ± 0.3% ΔF/F, n = 297, P < 0.0001; 10 kHz preferring: 1 kHz = 8.0 ± 0.5% ΔF/F, 5 kHz = 7.7 ± 0.5% ΔF/F, 10 kHz = 14.8 ± 0.8% ΔF/F, n = 169, P < 0.0001; 72 dB, 1 kHz preferring: 1 kHz = 14.2 ± 0.6% ΔF/F, 5 kHz = 8.4 ± 0.5% ΔF/F, 10 kHz = 3.9 ± 0.4% ΔF/F, n = 170, P < 0.0001; 5 kHz preferring: 1 kHz = 9.3 ± 0.4% ΔF/F, 5 kHz = 18.5 ± 0.6% ΔF/F, 10 kHz = 8.7 ± 0.5% ΔF/F, n = 331, P < 0.0001; 10 kHz preferring: 1 kHz = 7.0 ± 0.3% ΔF/F, 5 kHz = 12.0 ± 0.7% ΔF/F, 10 kHz = 19.4 ± 0.7% ΔF/F, n = 224, P < 0.0001, RM ANOVA; 1 kHz, 68 dB preferring: low = 14.1 ± 0.5% ΔF/F, high = 8.1 ± 0.3% ΔF/F, n = 390, P < 0.0001; 72 dB preferring: low = 7.7 ± 0.3% ΔF/F, high = 12.1 ± 0.4% ΔF/F, n = 323, P < 0.0001; 5 kHz, 68 dB preferring: low = 15.7 ± 0.6% ΔF/F, high = 10.7 ± 0.5% ΔF/F, n = 220, P < 0.0001; 72 dB preferring: low = 9.9 ± 0.3% ΔF/F, high = 16.8 ± 0.5% ΔF/F, n = 469, P < 0.0001; 10 kHz, 68 dB preferring: low = 15.0 ± 0.45 ΔF/F, high = 5.3 ± 0.4% ΔF/F, n = 381, P < 0.0001; 72 dB preferring: low = 7.8 ± 0.3% ΔF/F, high = 17.1 ± 0.5% ΔF/F, n = 344, P < 0.0001, paired, two-tailed t-test; somatosensory: 10 PSI preferring: 10 PSI = 15.2 ± 3.1% ΔF/F, 15 PSI = 7.1 ± 2.0% ΔF/F, 20 PSI = 10.4 ± 2.9% ΔF/F, n = 100, P < 0.0001; 15 PSI preferring: 10 PSI = 4.4 ± 0.9% ΔF/F, 15 PSI = 9.9 ± 1.1% ΔF/F, 20 PSI = 5.3 ± 0.8% ΔF/F, n = 69, P < 0.0001; 20 PSI preferring: 10 PSI = 14.3 ± 1.6% ΔF/F, 15 PSI = 13.3 ± 1.5% ΔF/F, 20 PSI = 24.5 ± 2.2% ΔF/F, n = 202, P < 0.0001, RM one-ANOVA).

(auditory: 68 dB, 1 kHz preferring: 5 kHz – control = 0.40 ± 0.02, DART = 0.62 ± 0.01, $P<0.0001$; 10 kHz – control = 0.38 ± 0.02, DART = 0.83 ± 0.02, $P < 0.0001$; 5 kHz preferring: 1 kHz – control

= 0.48 ± 0.02, DART = 0.61 ± 0.01, $P < 0.0001$; 10 kHz – control = 0.50 ± 0.01, DART = 0.61 ± 0.01, $P < 0.0001$; 10 kHz preferring: 1 kHz – control = 0.47 ± 0.02, DART = 0.52 ± 0.02, $P = 0.0505$; 5 kHz – control = 0.42 ± 0.02, DART = 0.49 ± 0.02, $P = 0.0149$; 72 dB, 1 kHz preferring: 5 kHz – control = 0.46 ± 0.02, DART = 0.55 ± 0.02, P = 0.0028; 10 kHz – control = 0.38 ± 0.02, DART = 0.30 ± 0.02, $P = 0.0031$; 5 kHz preferring: 1 kHz – control = 0.51 ± 0.02, DART = 0.53 ± 0.01, $P = 0.3230$; 10 kHz – control = 0.41 ± 0.02, DART = 0.49 ± 0.02, $P = 0.0120$; 10 kHz preferring: 1 kHz – control = 0.23 ± 0.01, DART = 0.40 ± 0.02, P < 0.0001; 5 kHz – control = 0.29 ± 0.02, DART = 0.63 ± 0.02, $P < 0.0001$; 1 kHz, 68 dB preferring: high – control = 0.41 ± 0.01, DART = 0.60 ± 0.01, $P < 0.0001$; 72 dB preferring: low – control = 0.50 ± 0.02, DART = 0.62 ± 0.01, $P < 0.0001$; 5 kHz, 68 dB preferring: high – control = 0.48 ± 0.01, DART = 0.69 ± 0.02, $P < 0.0001$; 72 dB preferring: low – control = 0.45 ± 0.02, DART = 0.61 ± 0.01, $P < 0.0001$; 10 kHz, 68 dB preferring: high – control = 0.39 ± 0.02, DART = 0.36 ± 0.02, $P = 0.1767$; 72 dB preferring: low – control = 0.32 ± 0.01, DART = 0.50 ± 0.01, $P < 0.0001$; somatosensory: 10 PSI preferring: 15 PSI – control = 0.23 ± 0.06, DART = 0.32 ± 0.04, $P = 0.2397$; 20 PSI – control = -0.20 ± 0.28, DART = 0.45 ± 0.04, $P = 0.0015$; 15 PSI preferring: 10 PSI – control = 0.11 ± 0.14, DART = 0.37 ± 0.04, $P = 0.0382$; 20 PSI – control = 0.00 ± 0.14, DART = 0.49 ± 0.04, $P = 0.0001$; 20 PSI preferring: 10 PSI – control = 0.29 ± 0.10, DART = 0.47 ± 0.02, $P = 0.0088$; 15 PSI – control = 0.27 ± 0.10, DART = 0.47 ± 0.02, $P = 0.0063$, unpaired t-test).

Supplemental Figure 10. Effects of DART on cells that are facilitated or unchanged by multisensory integration. a. Left, average time course of responses to uni- (tone: gray; puff: blue) and multisensory (tone + puff: green) stimuli for facilitated cells (subset matched to DART, n = 13). Error is SEM across cells. Right, amplitude of responses to tone, puff and tone + puff for all facilitated cells. **b.** Same as **a**, after DART infusion. **c.** Example cell that was modestly facilitated by the tone+puff (green) as compared to the puff alone (blue) in control conditions (left), and facilitation was greatly enhanced after DART infusion (right). **d.** Proposed cerebellar circuit mediating facilitation. **e-f.** Same as **a-b**, for unchanged cells (n = 11). Note that DART does not change the integration for these cells. *$p < 0.05$, **$p < 0.01$.

Supplemental Figure 11. **Local synaptic inhibition delays responses to all auditory stimuli tested.** Mean first (left) and peak (right) event times of significant trials before (black) and after (red) DART infusion for all individual cells with significant trial responses in both conditions. Overall mean ± SEM across cells overlaid. 1 kHz, 68 dB: n = 166 cells; 1 kHz, 72 dB: n = 101 cells; 5 kHz, 68 dB: n = 110 cells; 5 kHz, 72 dB: n = 188 cells; 10 kHz, 68 dB: n = 154 cells; 10 kHz, 72 dB: n = 157 cells; 3 mice.

Supplemental Figure 12. Local synaptic inhibition delays responses to auditory, but not somatosensory, stimuli. a. Mean first (left) and peak (right) event times of significant trials before (black) and after (red) DART infusion for all individual cells with significant trial responses to auditory stimuli in both conditions. Overall mean ± SEM across cells overlaid (n = 876). **b.** Same as **a**, for responses to air puffs (n = 104). ****$p < 0.0001$.

Supplemental Figure 13. Infusion of fluorescent muscimol in conditioned mice. Example widefield images of DAPI (left) and muscimol (right) fluorescence from three mice. Muscimol

injection was targeted at the floor of the primary fissure, spreading outward to include the anterior interpositus.

Supplemental Figure 14. Trained mice can distinguish pure tones. Individual mean CR probability (top) and amplitude (bottom) during CS+ trials and CS- trials with either a 1 kHz or 10 kHz tone. Overall mean ± SEM across mice overlaid (n = 4 mice). *$p < 0.05$, **$p < 0.01$.

Supplemental Figure 15. Blocking local synaptic inhibition does not change conditioned response kinematics. a. Average time courses of fractional eyelid closure (FEC) in response to conditioned stimuli that were either paired (CS+, top) or unpaired (CS-, bottom) with an unconditioned stimulus (US) after saline (black), nbDART (gray) or DART (red) infusion. Eyelid traces were averaged across mice **b.** Time of blink onset for all CRs in each condition for all CRs across mice (saline: n = 578, nb-DART: n = 327, DART: n = 339; RM ANOVA P < 0.0001, Tukey's multiple comparison's test: saline v. DART: P = 0.5837, saline v. nbDART: P < 0.0001, nbDART v. DART: P = 0.0015). Overall mean ± SEM across CRs overlaid. **c.** Summary of average time of blink onset for each mouse individually across conditions. Overall mean ± SEM across mice (n = 5) overlaid (RM ANOVA P = 0.2690). **d.** Same as **a**, for all 5 mice separately.

References

1. Strick, P.L., Dum, R.P. & Fiez, J.A. Cerebellum and nonmotor function. *Annu Rev Neurosci* **32**, 413-434 (2009).

2. Raymond, J.L. & Medina, J.F. Computational Principles of Supervised Learning in the Cerebellum. *Annu Rev Neurosci* **41**, 233-253 (2018).

3. Palay, S.L. & Chan-Palay, V. *Cerebellar cortex* (Springer, New York, 1974).

4. D'Angelo, E. & De Zeeuw, C.I. Timing and plasticity in the cerebellum: focus on the granular layer. *Trends Neurosci* **32**, 30-40 (2009).

5. Marr, D. A theory of cerebellar cortex. *J Physiol* **202**, 437-470 (1969).

6. Albus, J.S. A theory of cerebellar function. *Mathematical Biosciences* **10**, 25-61 (1971).

7. Chabrol, F.P., Arenz, A., Wiechert, M.T., Margrie, T.W. & DiGregorio, D.A. Synaptic diversity enables temporal coding of coincident multisensory inputs in single neurons. *Nat Neurosci* **18**, 718-727 (2015).

8. Huang, C.C.*, et al.* Convergence of pontine and proprioceptive streams onto multimodal cerebellar granule cells. *Elife* **2**, e00400 (2013).

9. Ishikawa, T., Shimuta, M. & Hausser, M. Multimodal sensory integration in single cerebellar granule cells in vivo. *Elife* **4** (2015).

10. Bengtsson, F. & Jorntell, H. Sensory transmission in cerebellar granule cells relies on similarly coded mossy fiber inputs. *Proc Natl Acad Sci U S A* **106**, 2389-2394 (2009).

11. Brickley, S.G., Cull-Candy, S.G. & Farrant, M. Development of a tonic form of synaptic inhibition in rat cerebellar granule cells resulting from persistent activation of GABAA receptors. *J Physiol* **497 (Pt 3)**, 753-759 (1996).

12. Rossi, D.J., Hamann, M. Spillover-mediated transmission at inhibitory synapses promoted by high affinity alpha-6 subunit GABAA receptors and glomerular geometry. *Neuron* **20**, 783-795 (1998).

13. Chadderton, P., Margrie, T.W. & Hausser, M. Integration of quanta in cerebellar granule cells during sensory processing. *Nature* **428**, 856-860 (2004).

14. Mitchell, S.J. & Silver, R.A. Shunting inhibition modulates neuronal gain during synaptic excitation. *Neuron* **38**, 433-445 (2003).

15. Wagner, M.J., Kim, T.H., Savall, J., Schnitzer, M.J. & Luo, L. Cerebellar granule cells encode the expectation of reward. *Nature* **544**, 96-100 (2017).

16. Giovannucci, A.*, et al.* Cerebellar granule cells acquire a widespread predictive feedback signal during motor learning. *Nat Neurosci* **20**, 727-734 (2017).

17. Knogler, L.D., Markov, D.A., Dragomir, E.I., Stih, V. & Portugues, R. Sensorimotor Representations in Cerebellar Granule Cells in Larval Zebrafish Are Dense, Spatially Organized, and Non-temporally Patterned. *Curr Biol* **27**, 1288-1302 (2017).

18. Ozden, I., Dombeck, D.A., Hoogland, T.M., Tank, D.W. & Wang, S.S. Widespread state-dependent shifts in cerebellar activity in locomoting mice. *PLoS One* **7**, e42650 (2012).

19. Deverett, B., Koay, S.A., Oostland, M. & Wang, S.S. Cerebellar involvement in an evidence-accumulation decision-making task. *Elife* **7** (2018).

20. Aller, M.I.*, et al.* Cerebellar granule cell Cre recombinase expression. *genesis* **36**, 97-103 (2003).

21. Chadderton, P., Margrie, T.W. & Ha, M. Integration of quanta in cerebellar granule cells during sensory processing. *Nature* **428**, 856-860 (2004).

22. Rancz, E.A.*, et al.* High-fidelity transmission of sensory information by single cerebellar mossy fibre boutons. *Nature* **450**, 1245-1248 (2007).

23. Henschke, J.U. & Pakan, J.M. Disynaptic cerebrocerebellar pathways originating from multiple functionally distinct cortical areas. *Elife* **9** (2020).

24. Chen, S., Augustine, G.J. & Chadderton, P. Serial processing of kinematic signals by cerebellar circuitry during voluntary whisking. *Nat Commun* **8**, 232 (2017).

25. Brown, S.T. & Raman, I.M. Sensorimotor Integration and Amplification of Reflexive Whisking by Well-Timed Spiking in the Cerebellar Corticonuclear Circuit. *Neuron* **99**, 564-575 e562 (2018).

26. Chen, S., Augustine, G.J. & Chadderton, P. The cerebellum linearly encodes whisker position during voluntary movement. *Elife* **5**, e10509 (2016).

27. Shambes, G.M., Gibson, J.M. & Welker, W. Fractured somatotopy in granule cell tactile areas of rat cerebellar hemispheres revealed by micromapping. *Brain Behav Evol* **15**, 94-140 (1978).

28. Proville, R.D.*, et al.* Cerebellum involvement in cortical sensorimotor circuits for the control of voluntary movements. *Nat Neurosci* **17**, 1233-1239 (2014).

29. Mathis, A.*, et al.* DeepLabCut: markerless pose estimation of user-defined body parts with deep learning. *Nat Neurosci* **21**, 1281-1289 (2018).

30. Cooke, S.F., Komorowski, R.W., Kaplan, E.S., Gavornik, J.P. & Bear, M.F. Visual recognition memory, manifested as long-term habituation, requires synaptic plasticity in V1. *Nat Neurosci* **18**, 262-271 (2015).

31. Heffley, W. & Hull, C. Classical conditioning drives learned reward prediction signals in climbing fibers across the lateral cerebellum. *Elife* **8** (2019).

32. Shields, B.C.*, et al.* Deconstructing behavioral neuropharmacology with cellular specificity. *Science* **356** (2017).

33. Duguid, I., Branco, T., London, M., Chadderton, P. & Häusser, M. Tonic Inhibition Enhances Fidelity of Sensory Information Transmission in the Cerebellar Cortex. *The Journal of Neuroscience* **32**, 11132-11143 (2012).

34. Isaacson, J.S. & Scanziani, M. How inhibition shapes cortical activity. *Neuron* **72**, 231-243 (2011).

35. Kalmbach, B.E., Voicu, H., Ohyama, T. & Mauk, M.D. A subtraction mechanism of temporal coding in cerebellar cortex. *J Neurosci* **31**, 2025-2034 (2011).

36. Kennedy, A.*, et al.* A temporal basis for predicting the sensory consequences of motor commands in an electric fish. *Nat Neurosci* **17**, 416-422 (2014).

37. Mauk, M.D. & Donegan, N.H. A model of Pavlovian eyelid conditioning based on the synaptic organization of the cerebellum. *Learn Mem* **4**, 130-158 (1997).

38. Fleming, E. & Hull, C. Serotonin regulates dynamics of cerebellar granule cell activity by modulating tonic inhibition. *J Neurophysiol* **121**, 105-114 (2019).

39. Straub, I.*, et al.* Gradients in the mammalian cerebellar cortex enable Fourier-like transformation and improve storing capacity. *Elife* **9** (2020).

40. Billings, G., Piasini, E., Lorincz, A., Nusser, Z. & Silver, R.A. Network structure within the cerebellar input layer enables lossless sparse encoding. *Neuron* **83**, 960-974 (2014).

41. Heiney, S.A., Wohl, M.P., Chettih, S.N., Ruffolo, L.I. & Medina, J.F. Cerebellar-dependent expression of motor learning during eyeblink conditioning in head-fixed mice. *J Neurosci* **34**, 14845-14853 (2014).

42. Liu, S.S. Differential conditioning and stimulus generalization of the rabbits nictitating membrane response. *J Comp Physiol Psychol* **77**, 136-142 (1971).

43. Siegel, S., Hearst, E., George, N. & O'Neal, E. Generalization gradients obtained from individual subjects following classical conditioning. *J Exp Psychol* **78**, 171-174 (1968).

44. Morissette, J. & Bower, J.M. Contribution of somatosensory cortex to responses in the rat cerebellar granule cell layer following peripheral tactile stimulation. *Exp Brain Res* **109**, 240-250 (1996).

45. Shimuta, M., Sugihara, I. & Ishikawa, T. Multiple signals evoked by unisensory stimulation converge onto cerebellar granule and Purkinje cells in mice. *Commun Biol* **3**, 381 (2020).

46. Jorntell, H. & Ekerot, C.F. Properties of somatosensory synaptic integration in cerebellar granule cells in vivo. *J Neurosci* **26**, 11786-11797 (2006).

47. Precht, W. & Llinas, R. Functional organization of the vestibular afferents to the cerebellar cortex of frog and cat. *Exp Brain Res* **9**, 30-52 (1969).

48. Tabuchi, S., Gilmer, J.I., Purba, K. & Person, A.L. Pathway-Specific Drive of Cerebellar Golgi Cells Reveals Integrative Rules of Cortical Inhibition. *J Neurosci* **39**, 1169-1181 (2019).

49. Gurnani, H. & Silver, R.A. Multidimensional population activity in an electrically coupled inhibitory circuit in the cerebellar cortex. *Neuron* **109**, 1739-1753 e1738 (2021).

50. Gilmer, J.I. & Person, A.L. Morphological Constraints on Cerebellar Granule Cell Combinatorial Diversity. *J Neurosci* **37**, 12153-12166 (2017).

51. Lanore, F., Cayco-Gajic, N.A., Gurnani, H., Coyle, D. & Silver, R.A. Cerebellar granule cell axons support high-dimensional representations. *Nat Neurosci* **24**, 1142-1150 (2021).

52. Cayco-Gajic, N.A., Clopath, C. & Silver, R.A. Sparse synaptic connectivity is required for decorrelation and pattern separation in feedforward networks. *Nature Communications* **8** (2017).

53. Cayco-Gajic, N.A. & Silver, R.A. Re-evaluating Circuit Mechanisms Underlying Pattern Separation. *Neuron* **101**, 584-602 (2019).

54. Rossi, P.*, et al.* Inhibition of constitutive inward rectifier currents in cerebellar granule cells by pharmacological and synaptic activation of GABA receptors. *Eur J Neurosci* **24**, 419-432 (2006).

55. Fore, T.R., Taylor, B.N., Brunel, N. & Hull, C. Acetylcholine Modulates Cerebellar Granule Cell Spiking by Regulating the Balance of Synaptic Excitation and Inhibition. *J Neurosci* **40**, 2882-2894 (2020).

56. Markwalter, K.H., Yang, Y., Holy, T.E. & Bonni, A. Sensorimotor Coding of Vermal Granule Neurons in the Developing Mammalian Cerebellum. *J Neurosci* **39**, 6626-6643 (2019).

57. Pouille, F. & Scanziani, M. Enforcement of temporal fidelity in pyramidal cells by somatic feed-forward inhibition. *Science* **293**, 1159-1163 (2001).

58. Kanichay, R.T. & Silver, R.A. Synaptic and cellular properties of the feedforward inhibitory circuit within the input layer of the cerebellar cortex. *J Neurosci* **28**, 8955-8967 (2008).

59. Duguid, I.*, et al.* Control of cerebellar granule cell output by sensory-evoked Golgi cell inhibition. *Proc Natl Acad Sci U S A* **112**, 13099-13104 (2015).

60. Crowley, J.J., Fioravante, D. & Regehr, W.G. Dynamics of fast and slow inhibition from cerebellar golgi cells allow flexible control of synaptic integration. *Neuron* **63**, 843-853 (2009).

61. Duguid, I., Branco, T., London, M., Chadderton, P. & Hausser, M. Tonic inhibition enhances fidelity of sensory information transmission in the cerebellar cortex. *J Neurosci* **32**, 11132-11143 (2012).

62. Safo, P. & Regehr, W.G. Timing dependence of the induction of cerebellar LTD. *Neuropharmacology* **54**, 213-218 (2008).

63. Ohyama, T., Nores, W.L., Murphy, M. & Mauk, M.D. What the cerebellum computes. *Trends Neurosci* **26**, 222-227 (2003).

64. Houck, B.D. & Person, A.L. Cerebellar Premotor Output Neurons Collateralize to Innervate the Cerebellar Cortex. *J Comp Neurol* **523**, 2254-2271 (2015).

65. Gao, Z.*, et al.* Excitatory Cerebellar Nucleocortical Circuit Provides Internal Amplification during Associative Conditioning. *Neuron* **89**, 645-657 (2016).

66. Khilkevich, A., Canton-Josh, J., DeLord, E. & Mauk, M.D. A cerebellar adaptation to uncertain inputs. *Sci Adv* **4**, eaap9660 (2018).

67. Perrett, S.P., Ruiz, B.P. & Mauk, M.D. Cerebellar cortex lesions disrupt learning-dependent timing of conditioned eyelid responses. *J Neurosci* **13**, 1708-1718 (1993).

68. Mittmann, W., Koch, U. & Hausser, M. Feed-forward inhibition shapes the spike output of cerebellar Purkinje cells. *J Physiol* **563**, 369-378 (2005).

69. Brown, A.M.*, et al.* Molecular layer interneurons shape the spike activity of cerebellar Purkinje cells. *Sci Rep* **9**, 1742 (2019).

70. Rudolph, S.*, et al.* Cerebellum-Specific Deletion of the GABAA Receptor delta Subunit Leads to Sex-Specific Disruption of Behavior. *Cell Rep* **33**, 108338 (2020).

71. Giovannucci, A.*, et al.* CaImAn an open source tool for scalable calcium imaging data analysis. *Elife* **8** (2019).

72. Pnevmatikakis, E.A. & Giovannucci, A. NoRMCorre: An online algorithm for piecewise rigid motion correction of calcium imaging data. *J Neurosci Methods* **291**, 83-94 (2017).

73. Pnevmatikakis, E.A.*, et al.* Simultaneous Denoising, Deconvolution, and Demixing of Calcium Imaging Data. *Neuron* **89**, 285-299 (2016).

74. Mathis, A.*, et al.* DeepLabCut: markerless pose estimation of user-defined body parts with deep learning. *Nat. Neurosci.* **21**, 1281-1289 (2018).

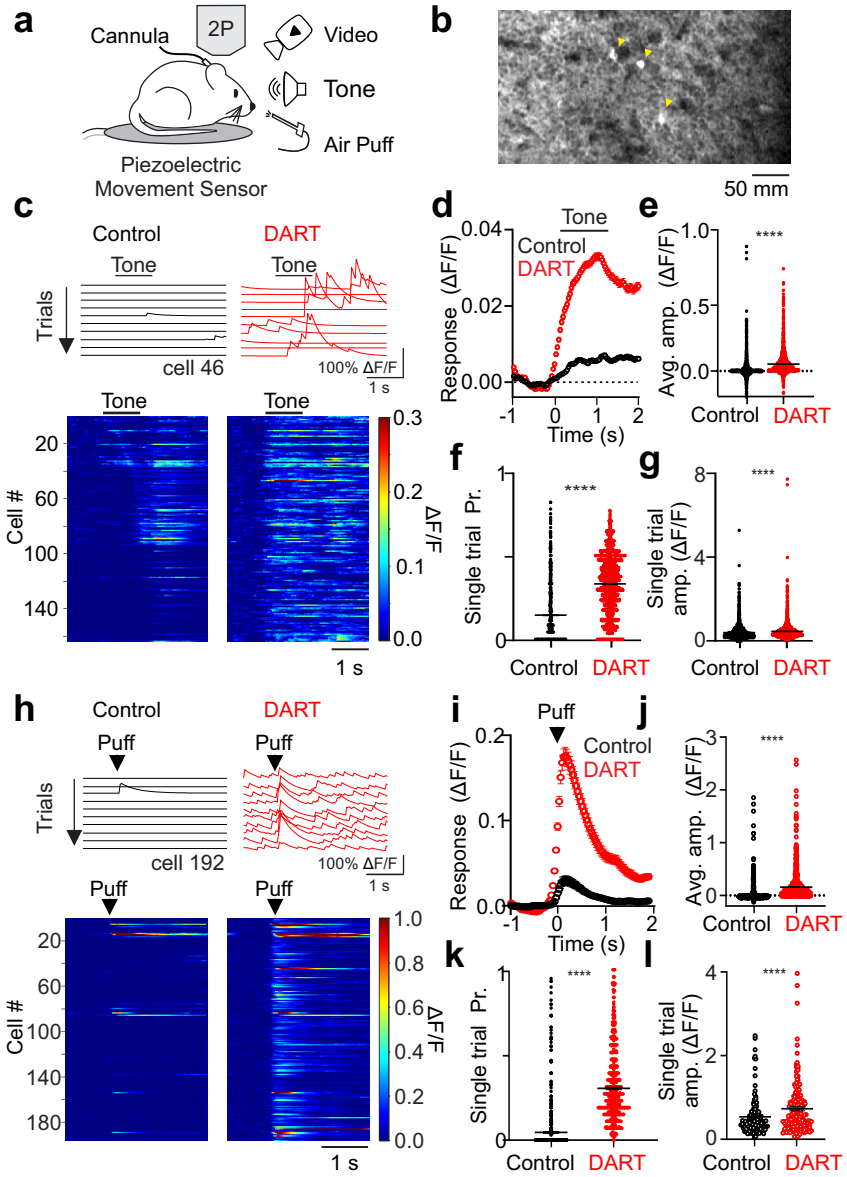
a
Cannula
2P
Video
Tone
Air Puff
Piezoelectric
Movement Sensor
b
50 mm
c
Control
DART
Tone
Trials
cell 46
100% ΔF/F
1 s
Cell #
ΔF/F
d
Response (ΔF/F)
Time (s)
e
Avg. amp. (ΔF/F)
Control
DART
f
Single trial Pr.
g
Single trial amp. (ΔF/F)
h
Puff
cell 192
i
j
k
l

Figure 1

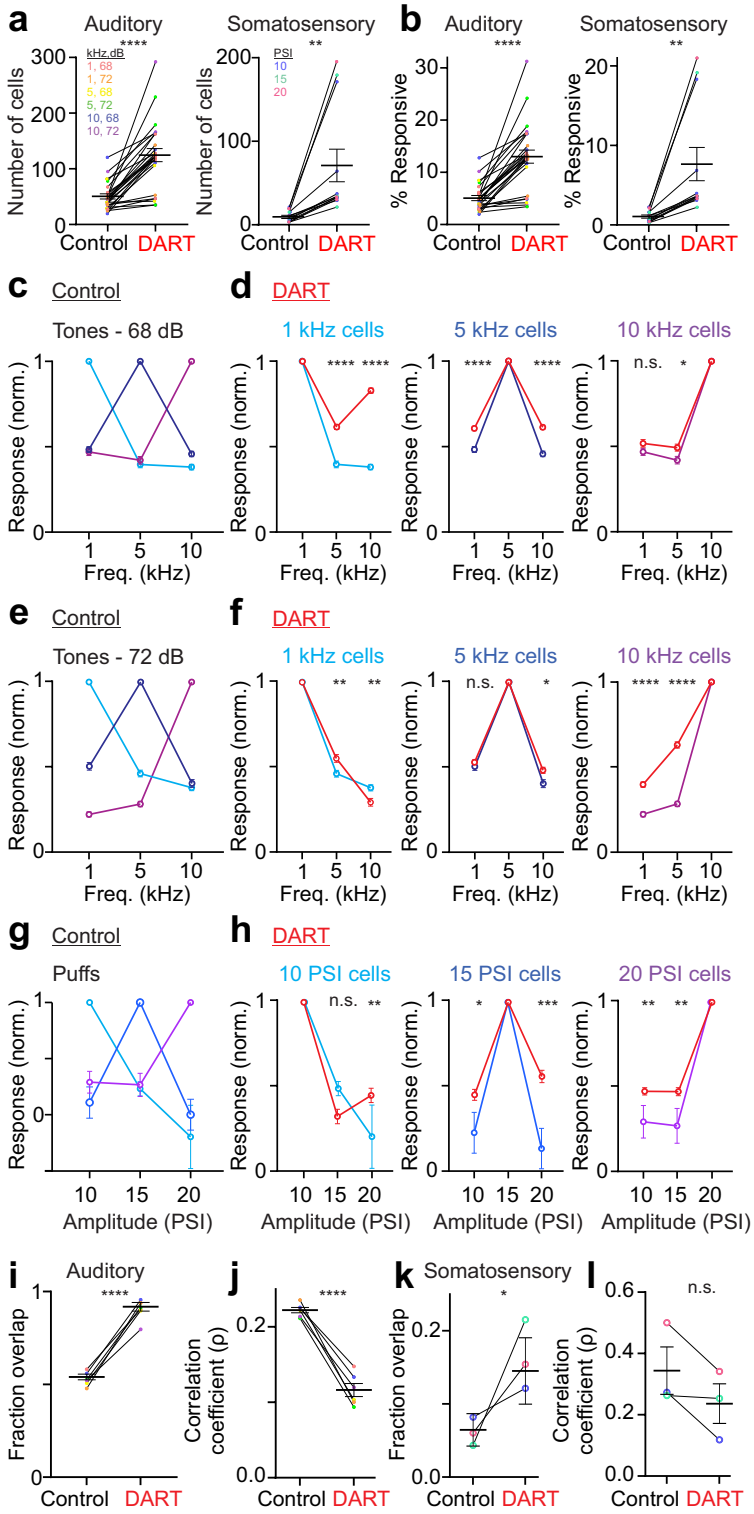
a
Auditory
Somatosensory
b
Auditory
Somatosensory
Number of cells
% Responsive
kHz,dB
1, 68
1, 72
5, 68
5, 72
10, 68
10, 72
PSI
10
15
20
Control
DART
c
Control
d
DART
Tones - 68 dB
1 kHz cells
5 kHz cells
10 kHz cells
Response (norm.)
Freq. (kHz)
e
Control
f
DART
Tones - 72 dB
1 kHz cells
5 kHz cells
10 kHz cells
g
Control
h
DART
Puffs
10 PSI cells
15 PSI cells
20 PSI cells
Amplitude (PSI)
i
Auditory
j
k
Somatosensory
l
Fraction overlap
Correlation coefficient (ρ)
n.s.

Figure 2

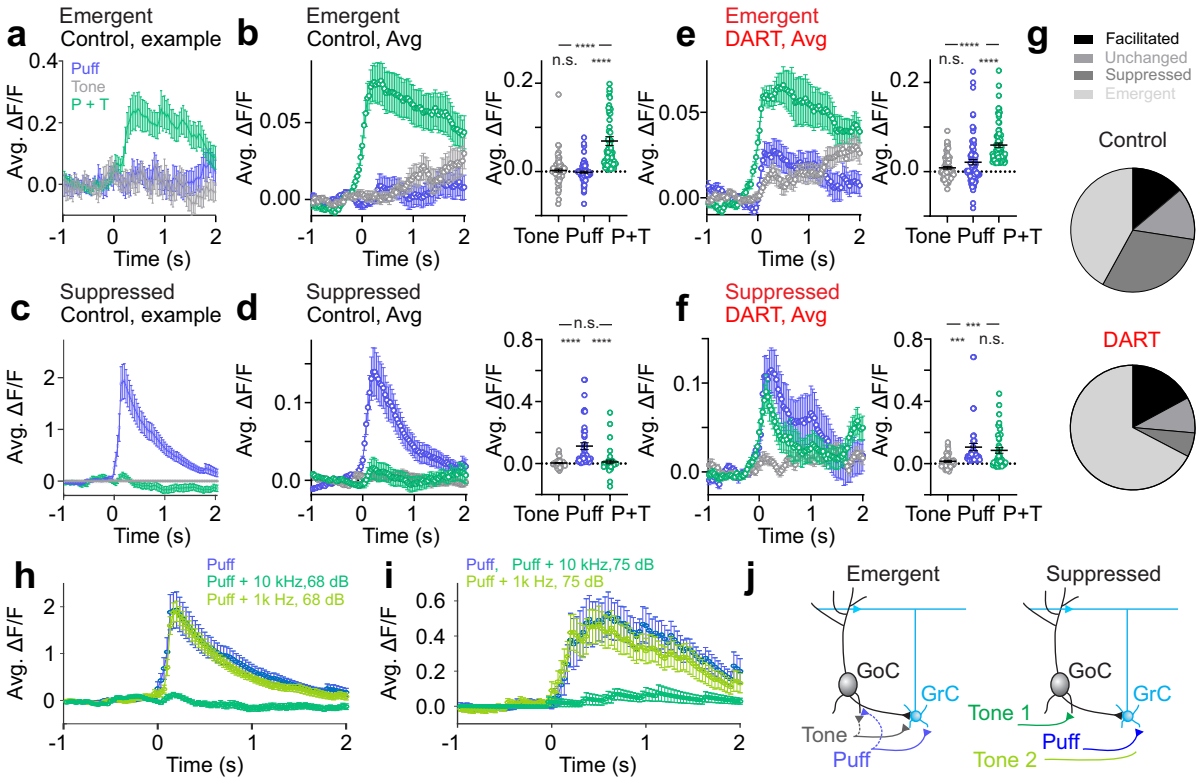
a
Emergent
Control, example
Puff
Tone
P + T
Avg. ΔF/F
Time (s)
b
Emergent
Control, Avg
Tone Puff P+T
n.s.
****
e
Emergent
DART, Avg
g
Facilitated
Unchanged
Suppressed
Emergent
Control
DART
c
Suppressed
Control, example
d
Suppressed
Control, Avg
f
Suppressed
DART, Avg
***
h
Puff
Puff + 10 kHz,68 dB
Puff + 1k Hz, 68 dB
i
Puff, Puff + 10 kHz,75 dB
Puff + 1k Hz, 75 dB
j
Emergent
Suppressed
GoC
GrC
Tone
Puff
Tone 1
Tone 2

Figure 3

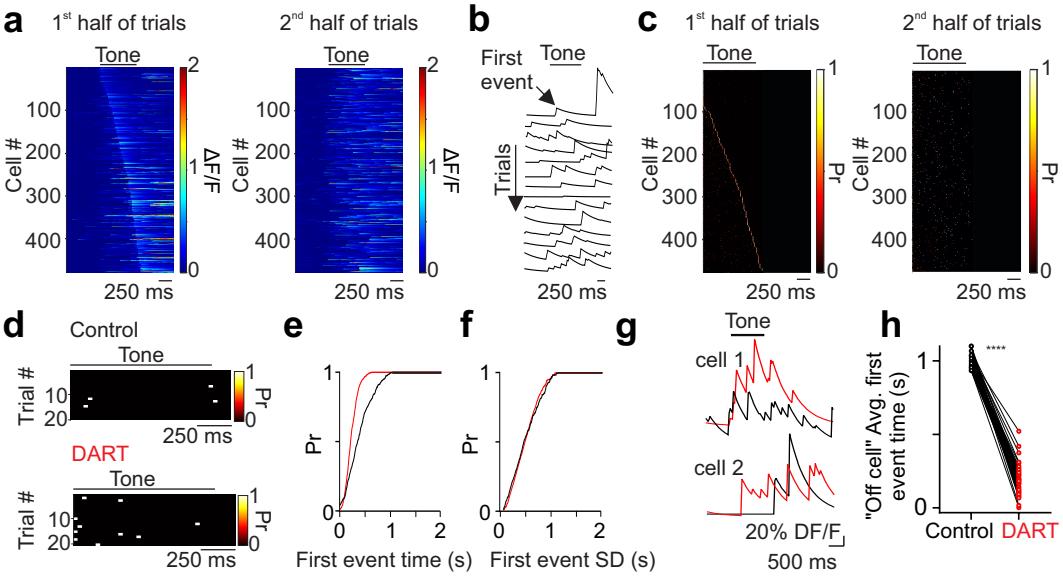
a
1st half of trials
2nd half of trials
Tone
Cell #
100
200
300
400
ΔF/F
2
1
0
250 ms
b
First event
Tone
Trials
250 ms
c
1st half of trials
2nd half of trials
Tone
Cell #
Pr
1
0
250 ms
d
Control
Tone
Trial #
10
20
Pr
250 ms
DART
e
Pr
First event time (s)
f
First event SD (s)
g
Tone
cell 1
cell 2
20% DF/F
500 ms
h
"Off cell" Avg. first event time (s)
****
Control
DART

Figure 4

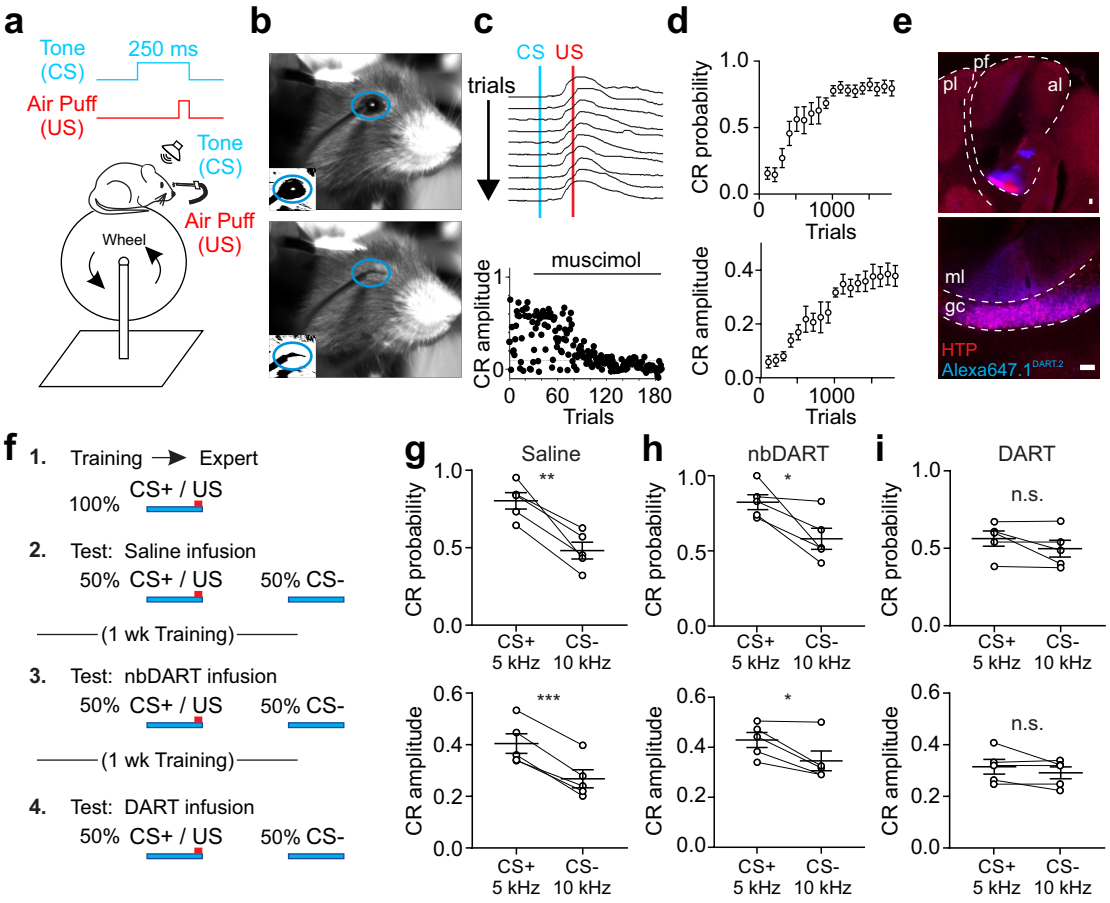
a
Tone (CS)
250 ms
Air Puff (US)
Tone (CS)
Air Puff (US)
Wheel
b
c
CS
US
trials
muscimol
CR amplitude
Trials
d
CR probability
Trials
CR amplitude
Trials
e
pf
pl
al
ml
gc
HTP
Alexa647.1
f
1. Training → Expert
100% CS+ / US
2. Test: Saline infusion
50% CS+ / US
50% CS-
(1 wk Training)
3. Test: nbDART infusion
50% CS+ / US
50% CS-
(1 wk Training)
4. Test: DART infusion
50% CS+ / US
50% CS-
g
Saline
h
nbDART
i
DART
CR probability
CR amplitude
CS+ 5 kHz
CS- 10 kHz
n.s.

Figure 5

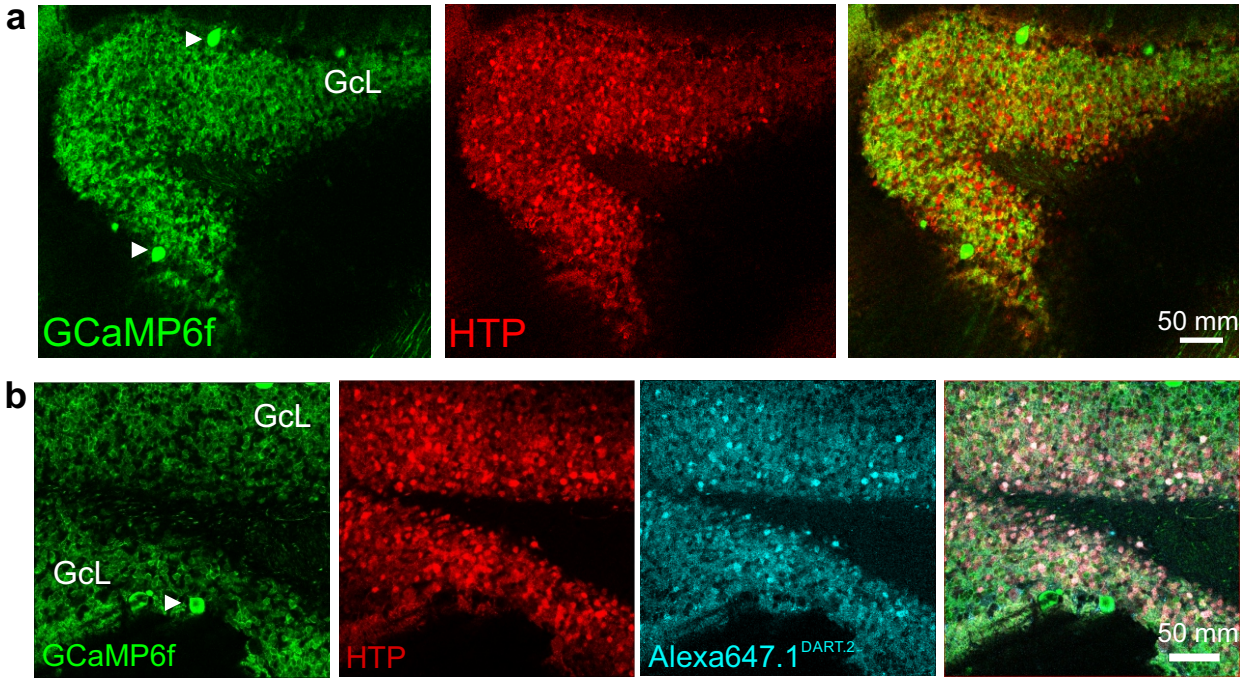

Supplemental Figure 1

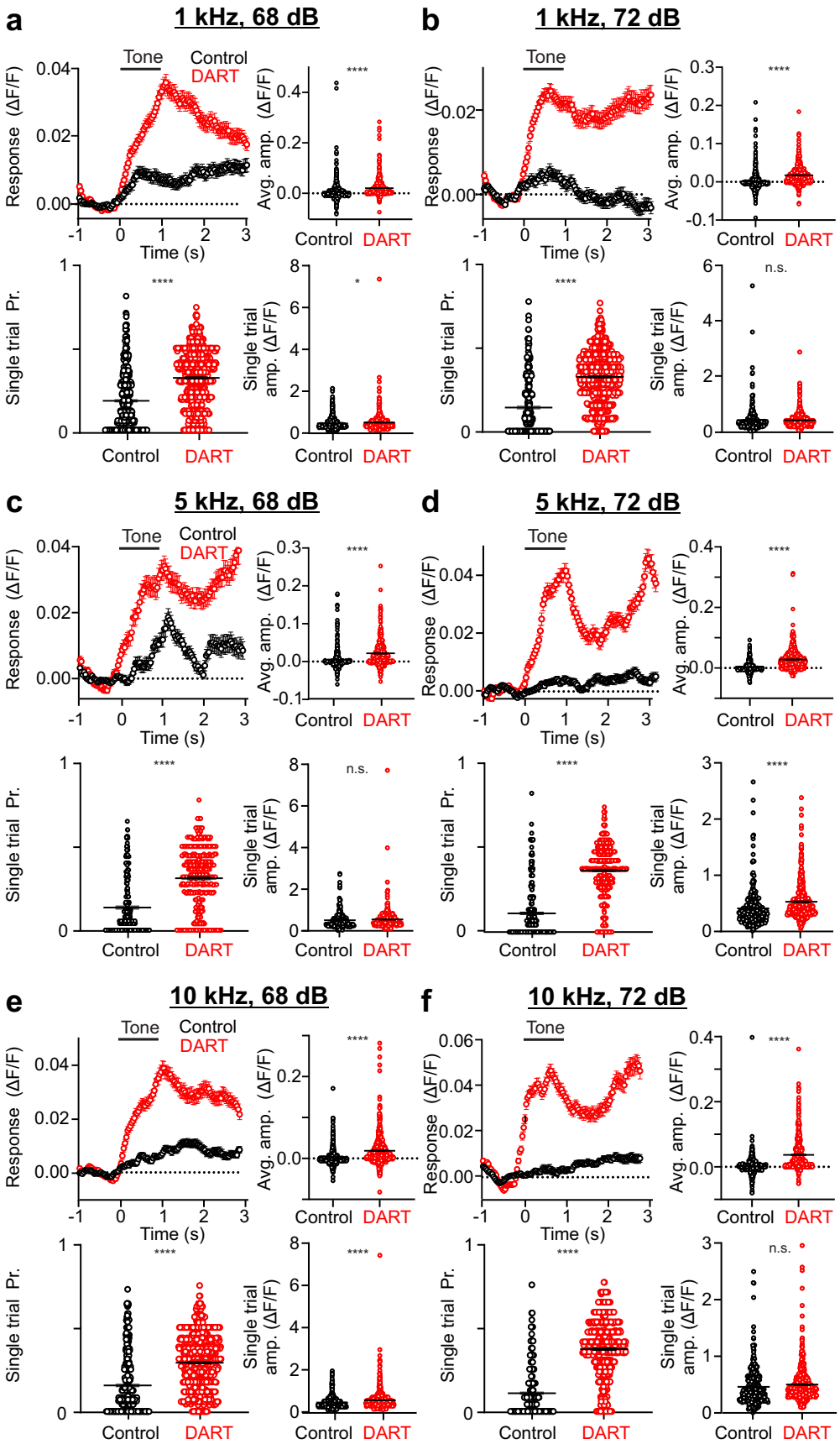

Supplemental Figure 2

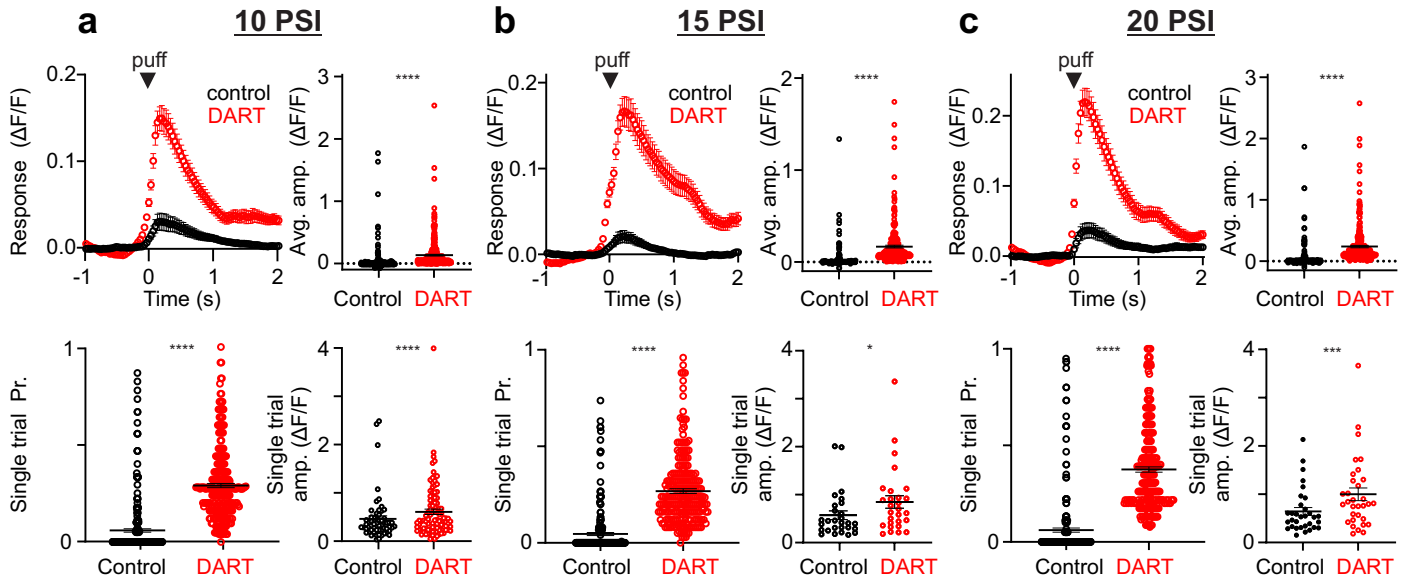

Supplemental Figure 3

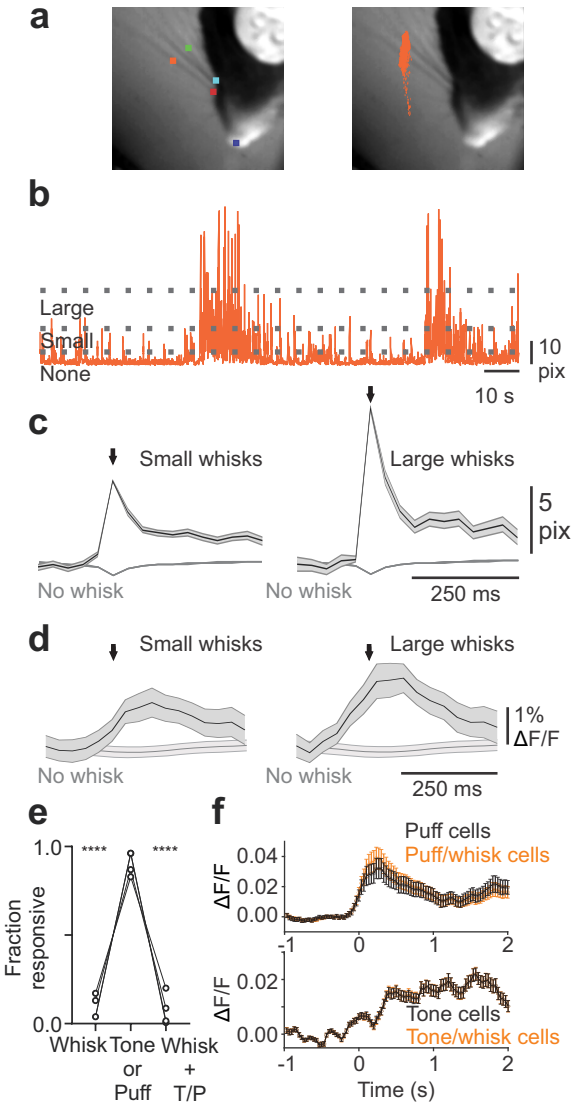

Supplemental Figure 4

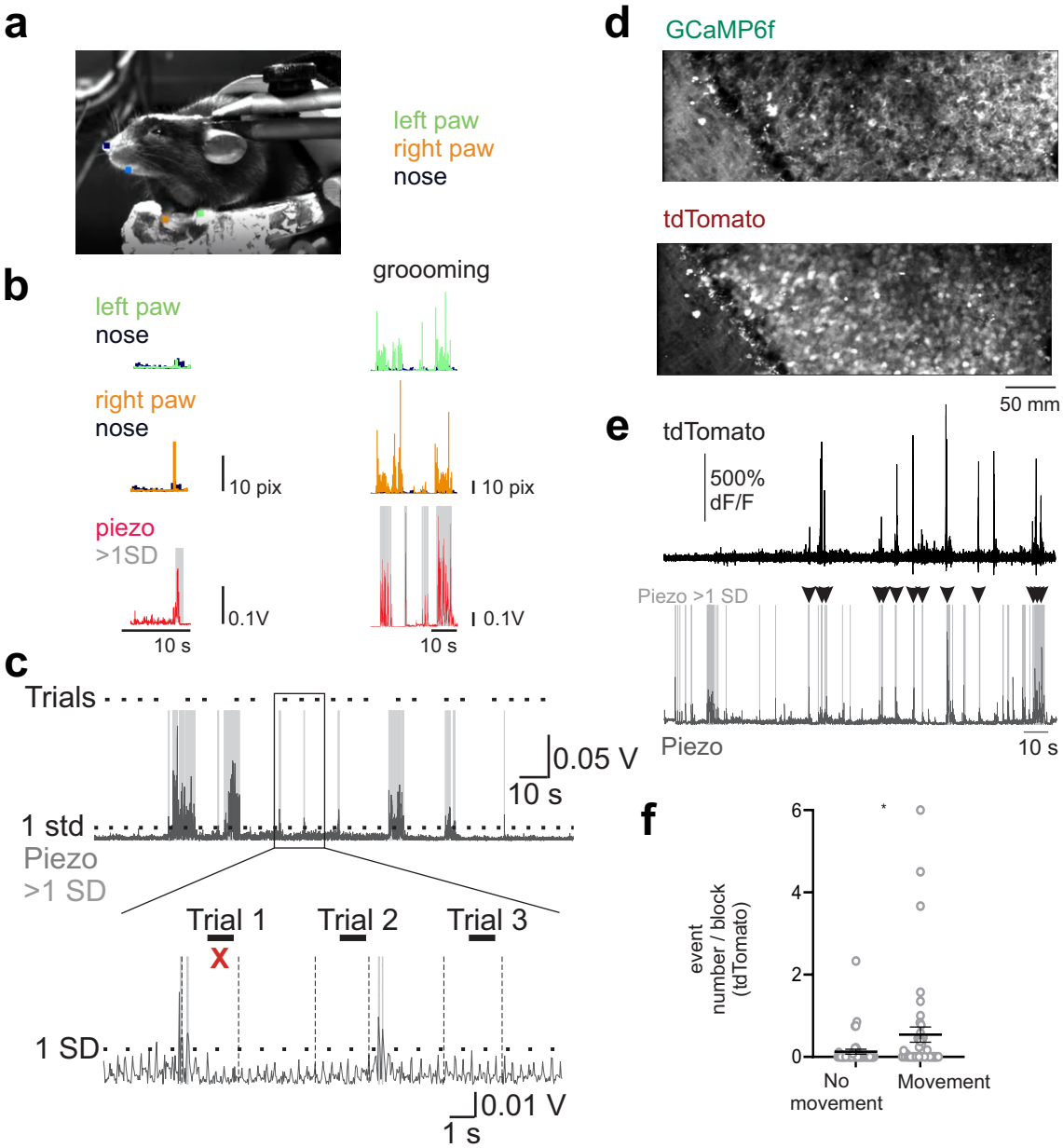

Supplemental Figure 5

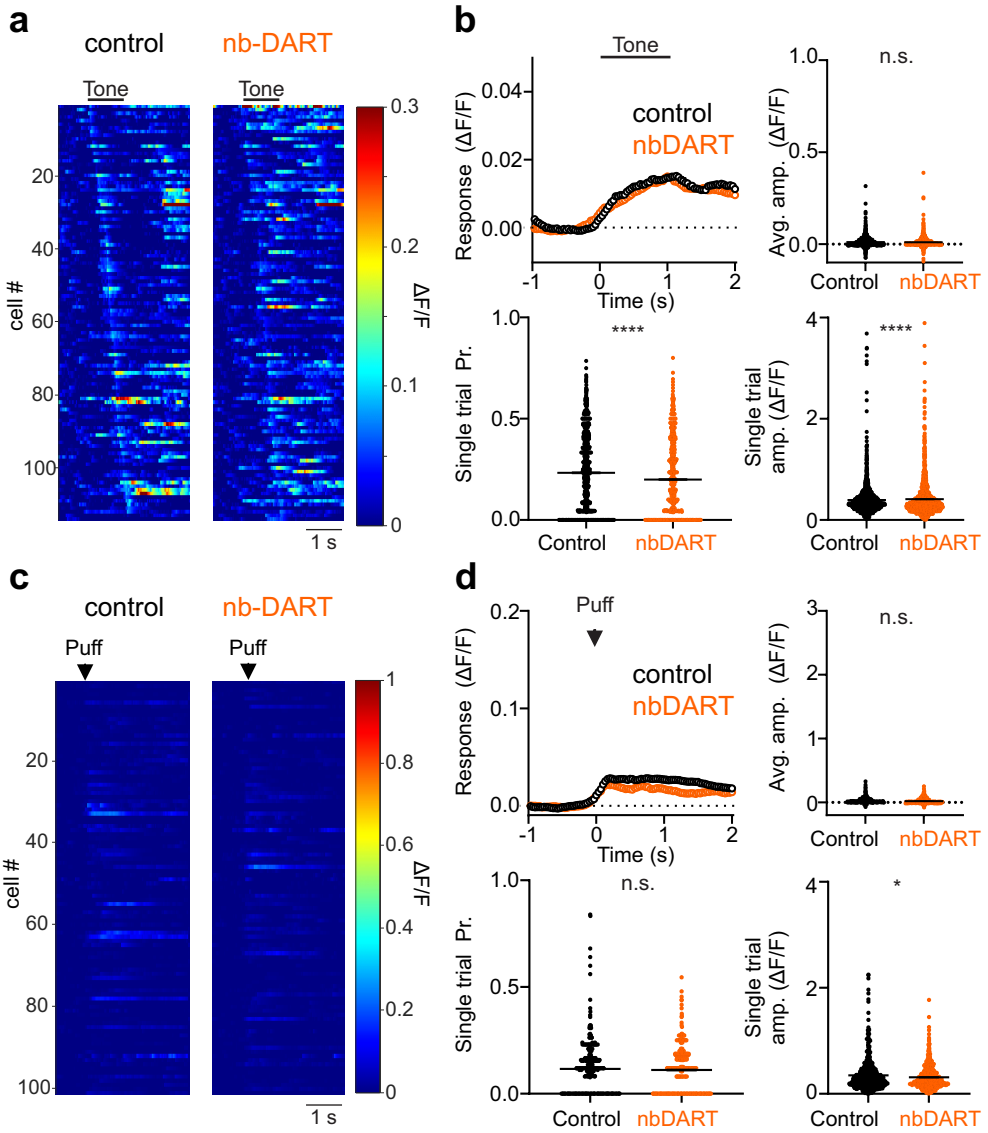

Supplemental Figure 6

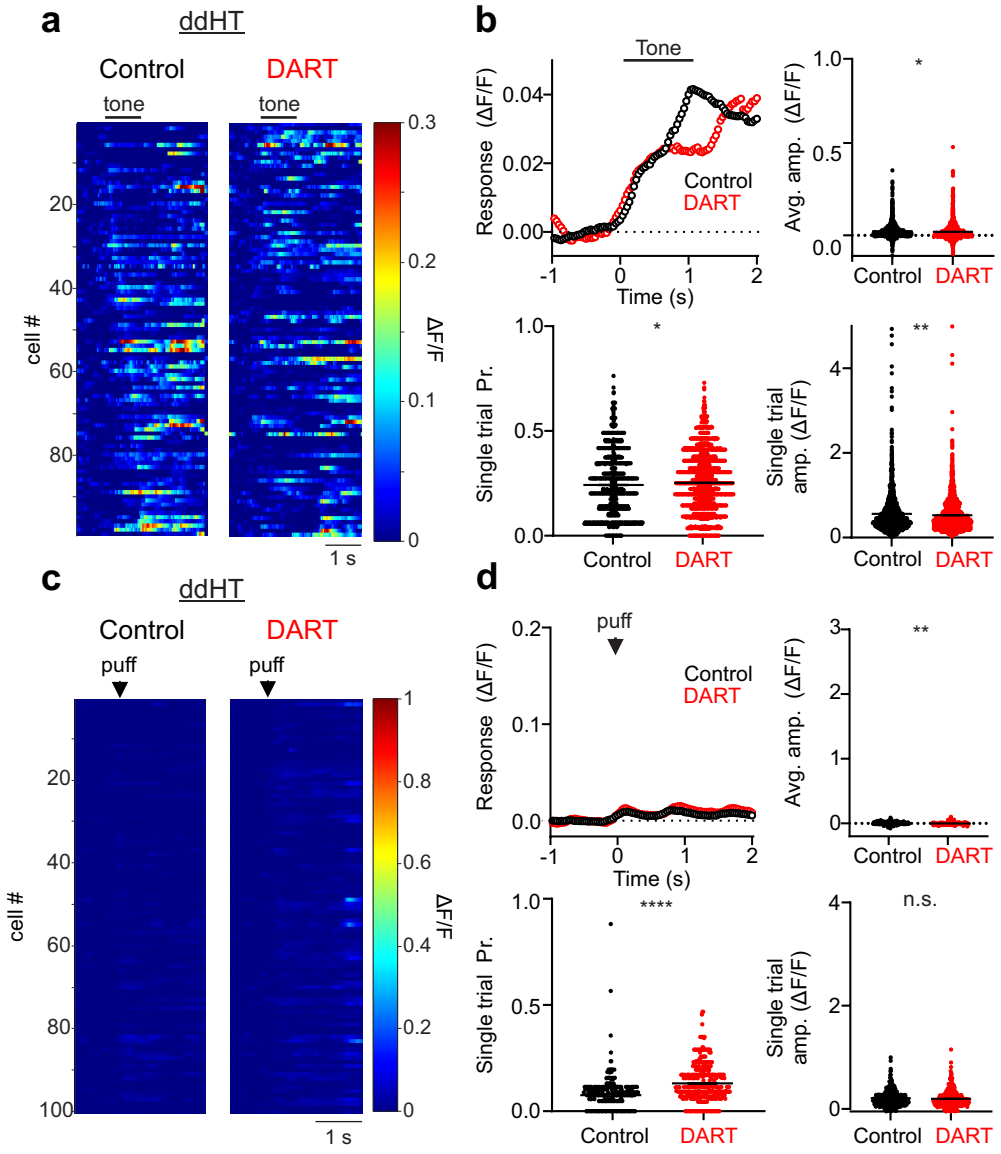

Supplemental Figure 7

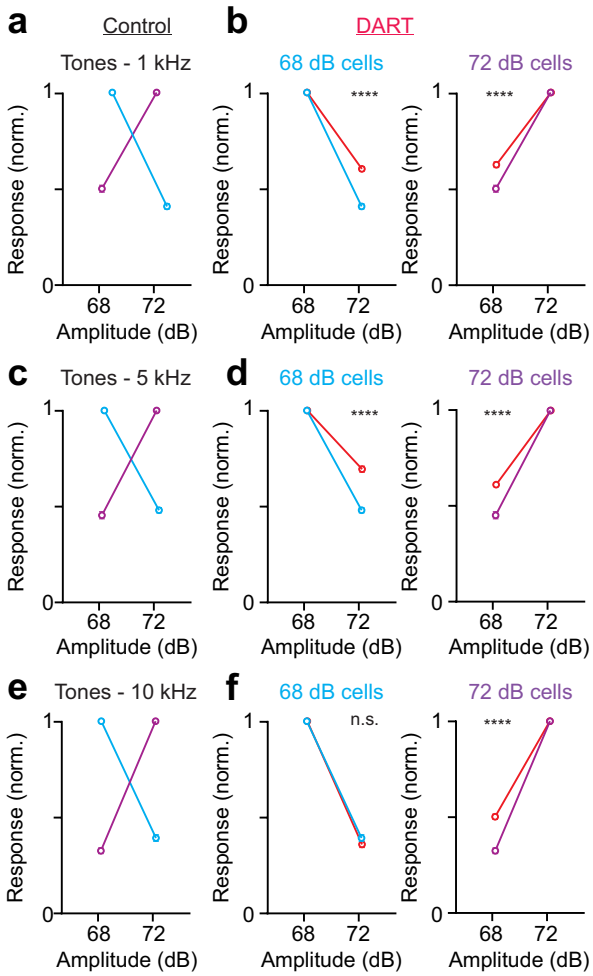

Supplemental Figure 8

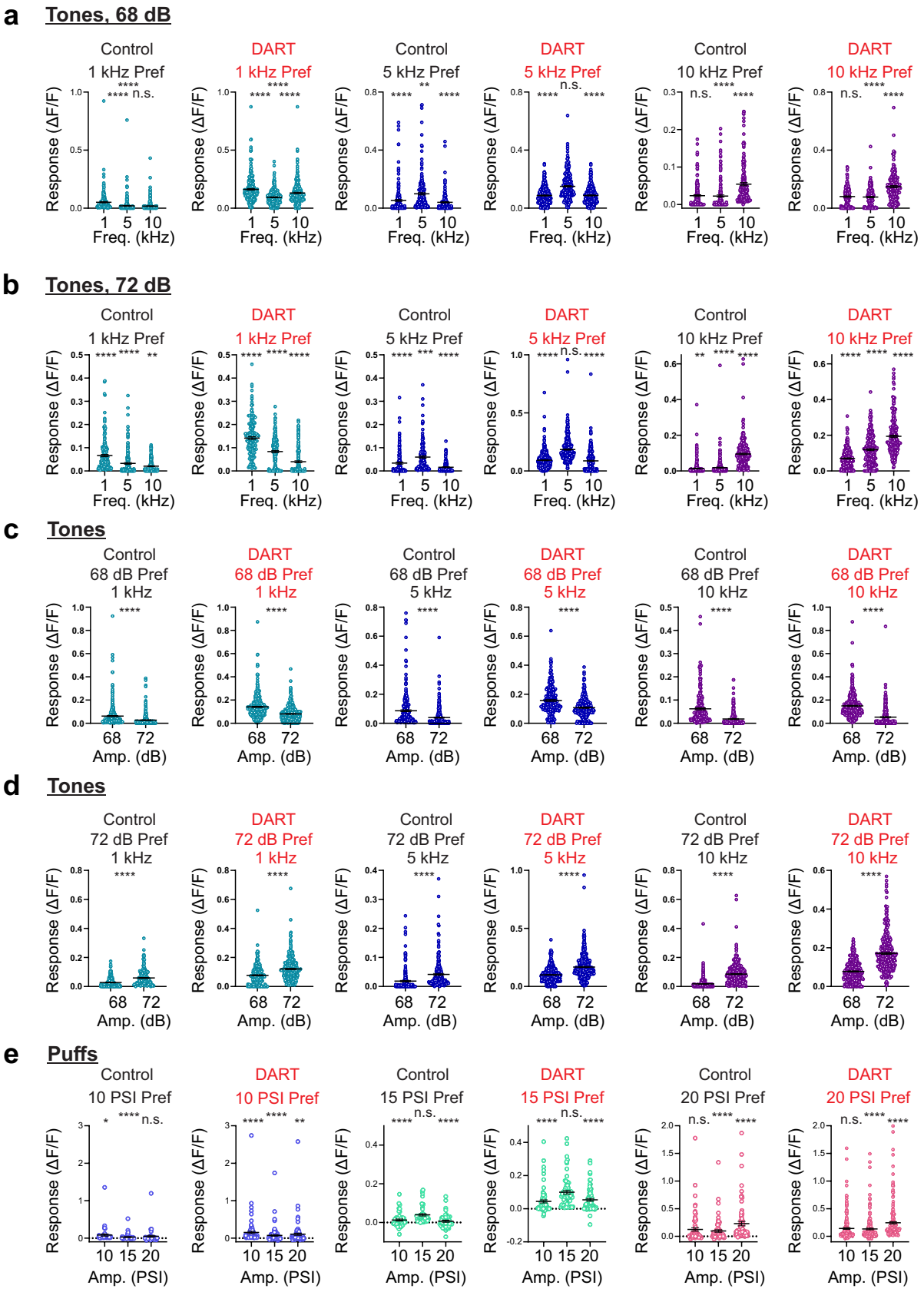

Supplemental Figure 9

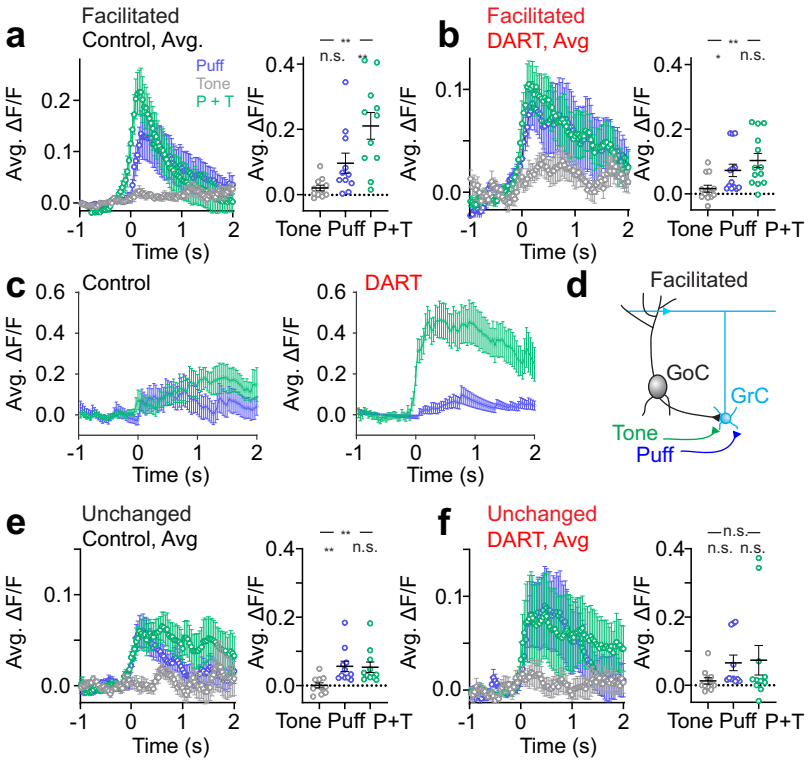

Supplemental Figure 10

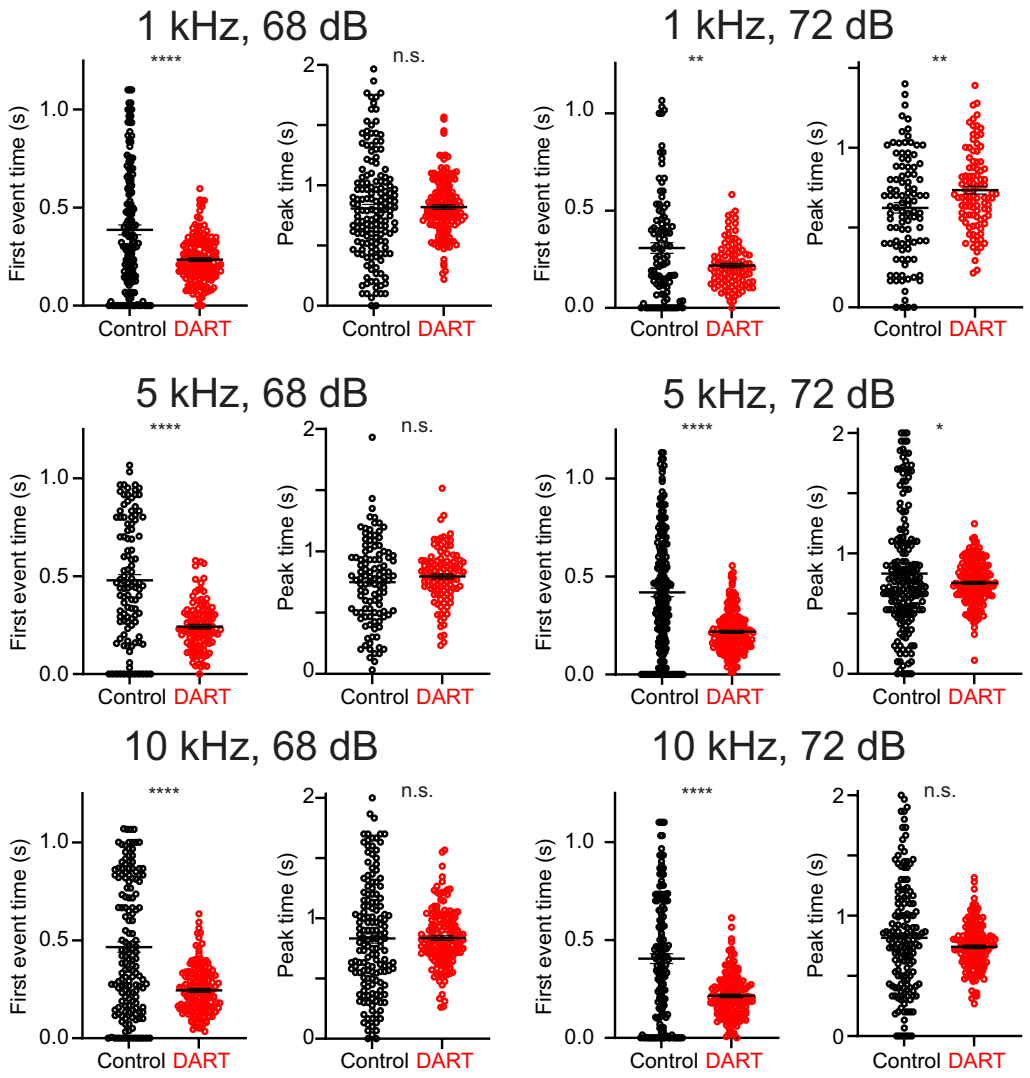

Supplemental Figure 11

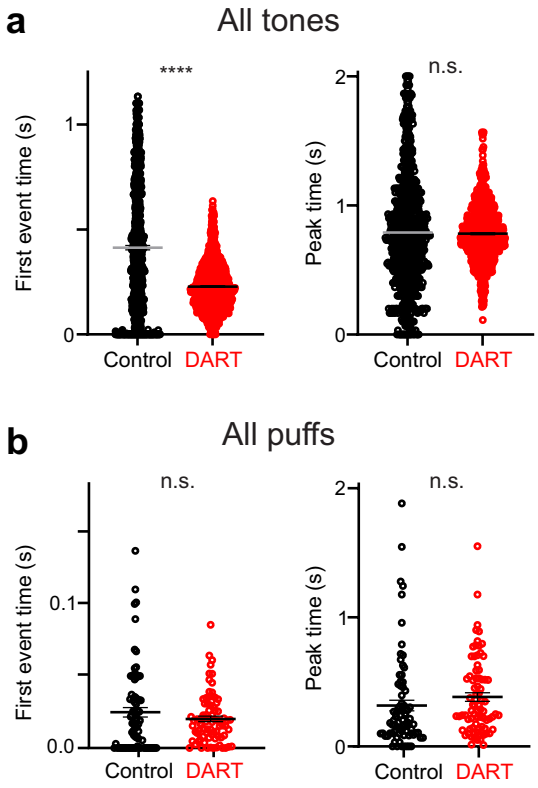

Supplemental Figure 12

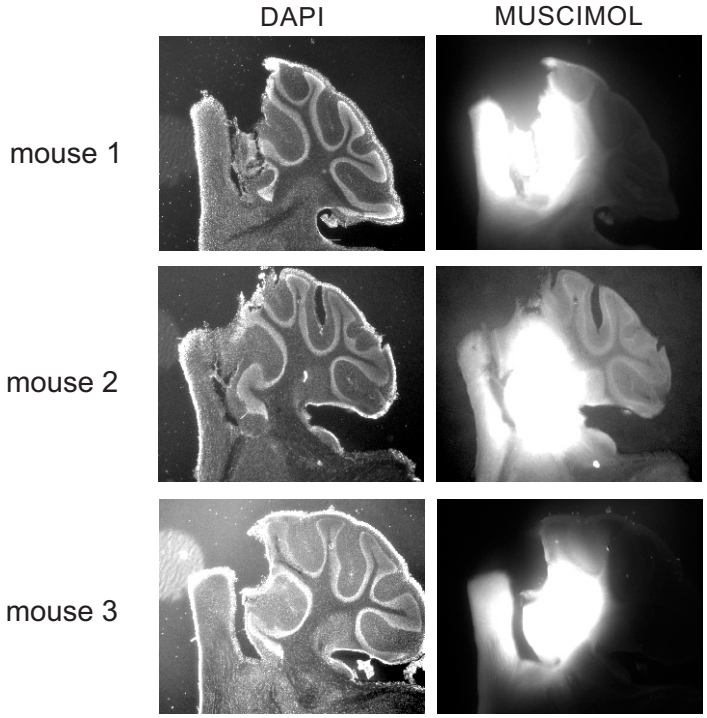

Supplemental Figure 13

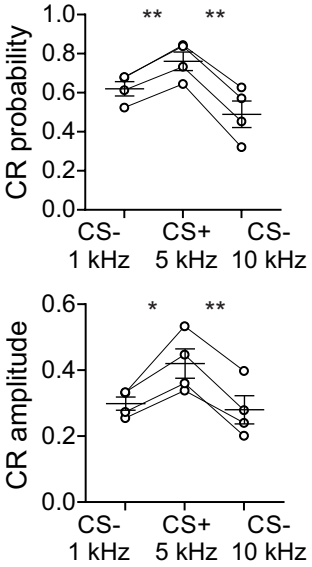

Supplemental Figure 14

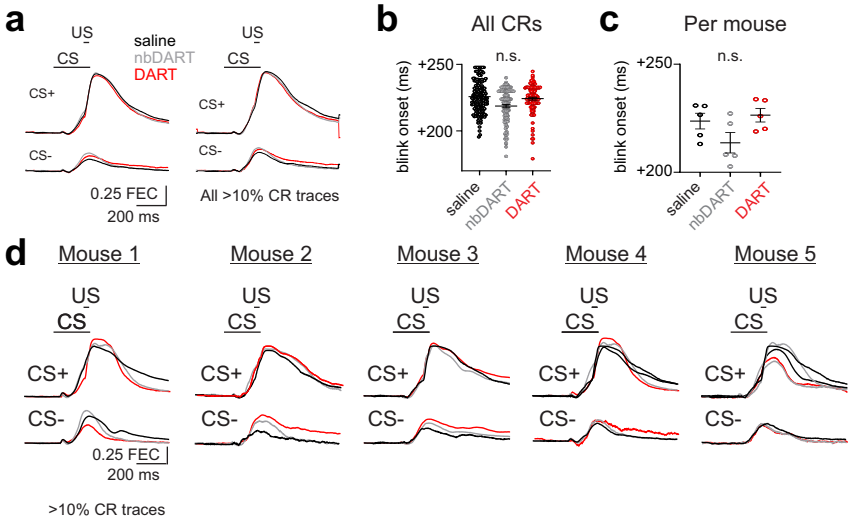

Supplemental Figure 15